

# Brittle tectonics in the western Arunachal Himalayan frontal fold belt, northeast India: Change in stress regime from pre-collisional extension to collisional compression

Tapos K. Goswami<sup>1</sup>  | Mousumi Gogoi<sup>1</sup>  | Bashab N. Mahanta<sup>2</sup>  |  
Soumyajit Mukherjee<sup>3</sup>  | Hiruj Saikia<sup>2</sup> | Mohamedharoon A. Shaikh<sup>4</sup>  |  
Pranjit Kalita<sup>1</sup> | Upendra Baral<sup>5</sup>  | Ranjan K. Sarmah<sup>1</sup>

<sup>1</sup>Department of Applied Geology, Dibrugarh University, Dibrugarh, India

<sup>2</sup>Geological Survey of India, Shillong, India

<sup>3</sup>Department of Earth Sciences, Indian Institute of Technology Bombay, Mumbai, India

<sup>4</sup>Department of Geology, The Maharaja Sayajirao University of Baroda, Vadodara, India

<sup>5</sup>Key Laboratory of Continental Collision and Plateau Uplift, Institute of Tibetan Plateau Research, Chinese Academy of Sciences, Beijing, China

## Correspondence

Tapos K. Goswami, Department of Applied Geology, Dibrugarh University, Dibrugarh -786004, Assam, India.  
Email: [taposgoswami@gmail.com](mailto:taposgoswami@gmail.com)

## Funding information

CPDA Grant IIT Bombay; International Geological Congress New Delhi

Handling Editor: A.K. Singh

The study of brittle deformation of the collisional mountains can explain its shallow crustal tectonic evolution and the palaeostress regime. The Main Boundary Thrust (MBT) zone in the western Arunachal Himalaya displays imbrication in the Permian Gondwana sequence between the MBT-1 (/Bome Thrust/MBT-Upper) in the north and MBT-2 (/MBT-Lower) in the south with consistent northerly dip. The Lower Gondwana rocks occur in the footwall of the MBT-1 with the Proterozoic Bomdila Group in the hangingwall. The upper Gondwana rocks constitute the hangingwall sequence for the MBT-2 with Neogene Siwalik rocks in the footwall. This article analyses palaeostress using brittle fractures in the Gondwana rocks that crop out for ~120 km<sup>2</sup> in the study area. The fault-bounded imbricate zone depicts eight brittle shear indicators and four sets of joints (J1 and J2: inclined and J3 and J4: subvertical). The signatures of the inherited pre-Himalayan extensional deformation are preserved in the Lower Gondwana Miri Formation. The Bichom and Bhareli rocks exhibit brittle deformation features of the Himalayan Orogeny under strong ~N-S compression. The palaeostress analysis of all joint sets indicates three phases of brittle deformation in the Gondwana and Siwalik rocks of the area. The subvertical joint sets and normal faults in the Miri Formation indicate a north-northwest (NNW)-directed extensional phase of the pre-Himalayan origin. The inclined joint sets of the Bichom and Bhareli formations of the Gondwana sequence depict Himalayan orogeny with ~N-S compressional phases. The third phase of brittle deformation in the Siwalik sequence depicts an east-west (~E-W) extension. The arc-parallel extension in the frontal fold belt of the Arunachal Himalaya may be due to oblique India-Asia collisional tectonics.

## KEYWORDS

convergent setting, deformation mechanism, shear kinematics, stress regime

## 1 | INTRODUCTION

The continental collision between the Indian and Asian plates took place ~55 Ma ago (Hodges, 2000; Yin, 2006; Mukherjee, Puneekar, Mahadani, & Mukherjee, 2015). The post-collisional crustal shortening was

accommodated through a number of near-parallel to north-dipping thrusts in the Himalaya. Towards the south, these are the Main Central Thrust (MCT), the Main Boundary Thrust (MBT), and the Main Frontal Thrust (MFT; Yin, 2006; Figure 1a). The Indian Plate is currently moving towards the NE direction at a rate of ~50 mm/year (Keary, Klepeis, &

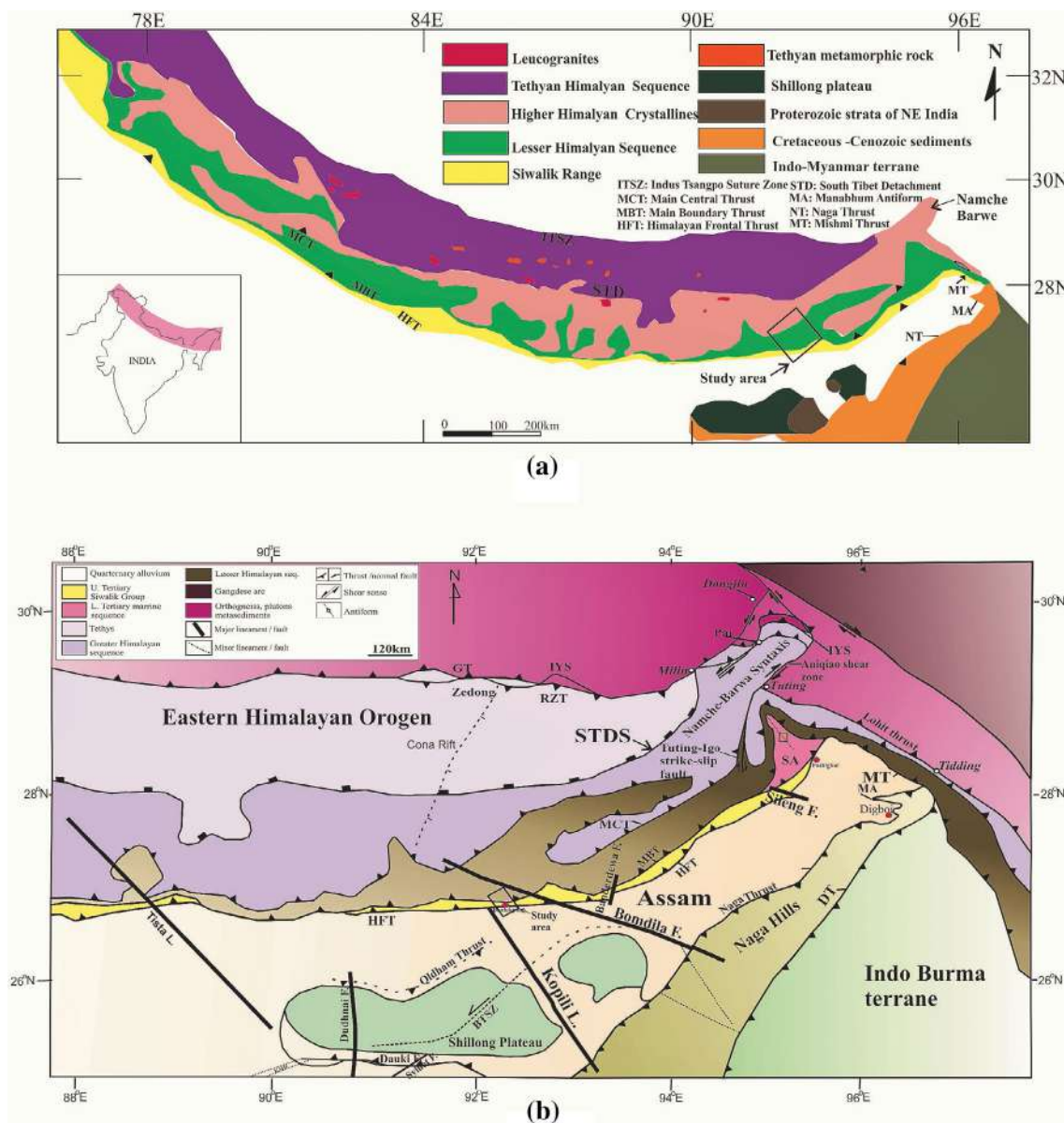


**FIGURE 1** (a) Geological map of the Himalayan orogen (modified from Yin et al., 2010b). The location of the area of study in Arunachal Himalaya is shown. (b) The geological map of eastern Himalaya (modified from Ding, Zhong, Yin, Kapp, & Harrison, 2001). The study area is shown by a rectangle. Namche Barwa Syntaxis is shown along with Tuting-Igo strike-slip fault. The orogen subparallel Bomdila Fault and orogen transverse Kopili Fault are shown. DT, Dishang Thrust; GT, Gangdese Thrust; HFT, Himalayan Frontal Thrust; IYS, Indus Yalu Suture; MBT, Main Boundary Thrust; MCT, Main Central Thrust; MT, Mishmi Thrust; NT, Naga Thrust; RZT, Renbu Zedong Thrust; SA, Siang Antiform; STDS, South Tibet Detachment System

Vine, 2009) with respect to the Eurasian Plate. The ongoing deformation is manifested by seismicity along with the MCT, MBT, and MFT (Rajendran, Parameswaran, & Rajendran, 2017).

In Bhutan and Arunachal Indian Himalaya, a number of recent earthquakes indicate shallow focal depth and the hypocenters restricted within the zone of MCT and MBT (Baruah & Kayal, 2013; Kayal, 1996 and references therein). Furthermore, a major orogen-transverse strike-slip fault in the region, the Kopili Fault is also responsible for major earthquakes (Mw 6 and 5.1, in 2009) in Bhutan and Assam (Kayal, et al., 2010). Recurring

earthquakes in the eastern Himalaya reveal that the northwestern (NW) part of the Bomdila Fault is seismogenic (Sarma & Sharma, 2018; Sharma, Sarma, & Baruah, 2018; Figure 1b). The interface of the strike-slip Kopili Fault and the MFT received much attention in recent years due to the shallow-focus earthquakes (Mukhopadhyay, Riguzzi, Mullick, & Sengupta, 2020). The causative stress regime for these earthquakes is provided through focal mechanism solutions. However, geoscientists need to know the stress regime in the geologic past to understand the tectonics of the region more explicitly.

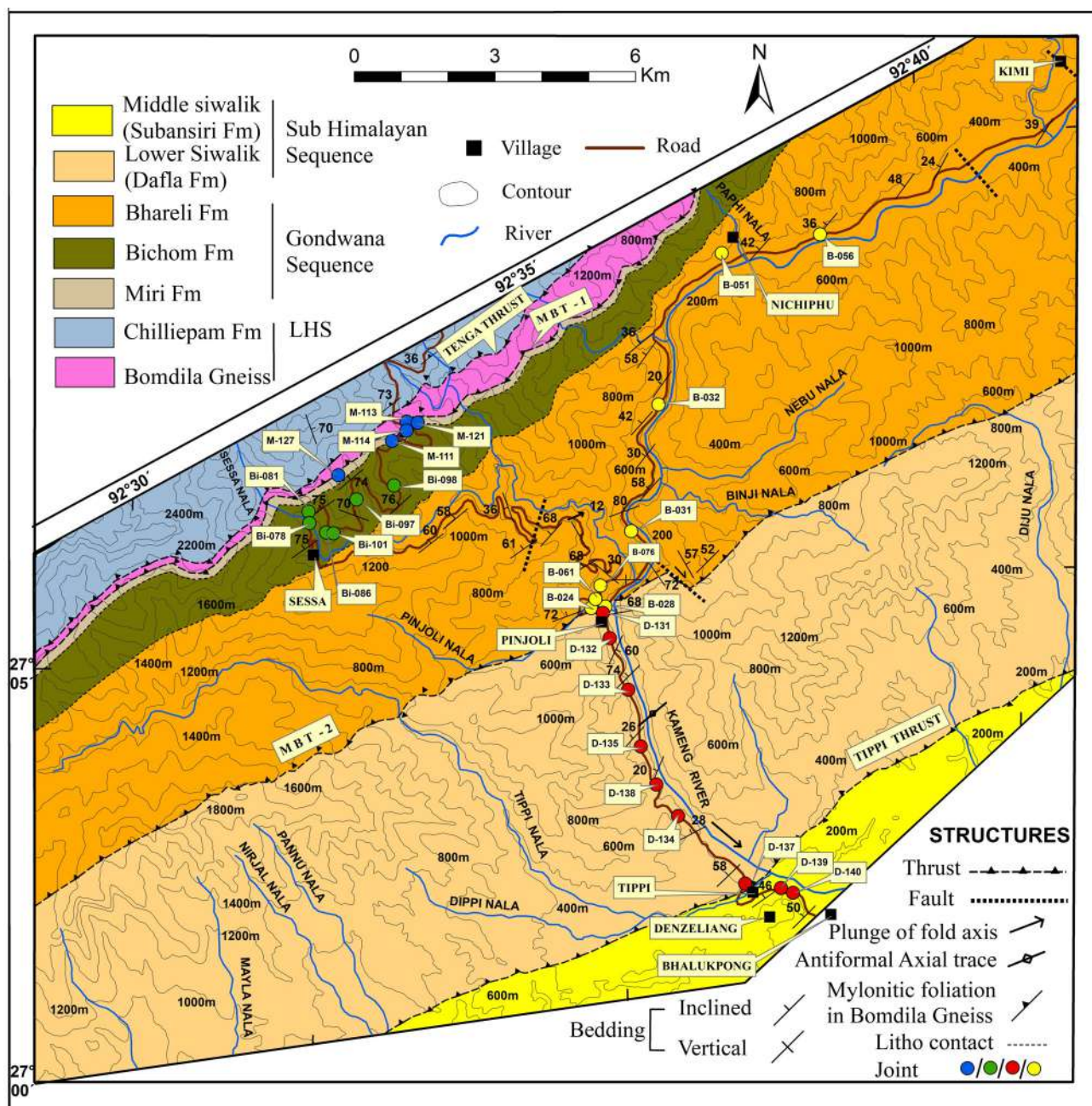


**FIGURE 2** Geological map of the area (modified from Bhukosh database, GSI) of the Pinjoli-Sessa-Nichiphu-Kimi-Bhalukpong area. MBT-1 between the Bomdila and Gondwana Group of rocks and MBT-2 between the Gondwana and Siwalik Group of rocks are shown. Bedding attitudes are shown with joint plane data points. Solid circle blue with prefix M are the data from Miri Formation; solid circle green with prefix Bi are data points for the Bichom Formation. Solid circle yellow with prefix B are data points for Bhareli Formation and solid circle red with prefix D are data points for Siwalik Group of rocks

Palaeoseismological study in the frontal Mishmi Ranges had an estimated dip-slip of  $24.6 \pm 4.6$  m for a  $25 \pm 5^\circ$ E dipping fault during the 1950 Assam earthquake (Singh et al., 2021). Interestingly, the 1950 earthquake nucleated further east of the Tuting-Tidding Suture Zone, where the locked zone that demarcates the brittle and ductile segments of Main Himalayan Thrust (MHT) occurs. This is unlike the rest of the Himalaya where the locked zone of the MHT is generally located beneath the topographic front of the Higher Himalaya. Across the ~65-km-wide seismo-potential locked zone of the Mishmi Range,

a global positioning system (GPS) convergence rate of 20 mm/year was proposed (Devachandra, Kundu, Catherine, Kumar, & Gahalaut, 2014). If it is assumed that all previously accumulated inter-seismic strain was released by the 1950 Assam earthquake ( $M_w$  8.6), a slip deficit of ~1.4 m is capable of generating an  $M_w$  ~ 7.7 earthquake along the Mishmi Thrust in the present day (Singh et al., 2021). Furthermore, a calculated dip-slip of  $15.3 \pm 4.6$  m is demonstrated to be due to the rupture produced by the great 1,697 CE Sadiya earthquake. The magnitude of this earthquake is estimated to be between

$M_w$  7.7–8.1 and the minimum rupture length of this earthquake is calculated to be ~100 km (Pandey et al., 2021).

Along the strike of the Himalayan orogen, the hanging wall and the footwall sequences across the MBT are intensely deformed. Changes in the intensity and orientation of the compressive stresses during the evolution of the orogen are documented through numerous deformation structures (Shah, Srivastava, & Joshi, 2012 and references therein). In the Darjeeling Himalaya, the MBT sheet has been folded and rotated due to the slip along the south Kalijora Thrust (SKT) in the footwall (Mukul, 2000). The MBT footwall imbrications in the north of the SKT developed splays. Movement along these splays is responsible for the uplift of the gravel beds and strath terraces along the folded trace of the MBT zone. The SKT sheet is modified by the formation of connecting splay duplexes which have caused the MBT Fault propagation-related antiform to become open and the synform overturned with the limbs dipping southerly.

In the northwestern Himalaya, within the Mohand Range in the south of MBT, the MFT sheet depicts fault propagation folding. It is interpreted that MFT is an emergent fault and the folds formed first at the propagating MFT tip, then these folds were subsequently dismembered by the MFT itself. From the optically stimulated luminescence (OSL) dating, it is observed that MFT evolved in segments in the Mohand Range. From the OSL age of the uplifted Quaternary sediments, the youngest MFT activity in the region is constrained to be <15 ka (Srivastava, Mukul, & Barnes, 2016; Srivastava, Mukul, Barnes, & Mukul, 2018). Based on Fission Track thermochronological studies from the Kumaun region by Singh and Patel (2021), MBT was developed during the Late Miocene (i.e., ~13 Ma) and reactivated along with associated faults around the Plio–Pleistocene. In Uttarakhand, the Siwalik rocks between the MFT and MBT are incised

by three thrust planes. Among these, the Bhauwala Thrust and Santaugarh Thrust are reported to be active (Jayangondaperumal, Thakur, Joevivek, Rao, & Gupta, 2018) and therefore have been considered as out-of-sequence thrusts (review in Mukherjee et al., 2015). The Siwalik rocks are folded into anticlines and synclines (Thakur & Pandey, 2004; Wesnousky, Kumar, Mahindra, & Thakur, 1999). Eight strike-slip faults are reported from the area and the trend of these faults are N-S, north-northeast (NNE)–south-southwest (SSW), and NE-SW (Dutta, Biswas, & Mukherjee, 2019; Jayangondaperumal, Dubey, & Sen, 2010). Based on small-scale brittle slip directions, an attitude of the near-vertical and inclined joint sets, an arc-parallel compression in the Siwalik Himalaya is proposed based on palaeostress analysis (Dutta et al., 2019).

The eastern Himalayan Permian Gondwana sediments are deformed along with the MBT and the brittle deformation of the Gondwana sequence may be synchronous with the deposition of the Siwalik sediments in the south. The deposition of sediments in the Siwalik molasse basin is dated as ~13 Ma and deformation of the Gondwana sequence in the north might have continued through the Neogene Siwalik sequence to the Quaternary alluvium across the Himalayan Frontal Thrust (HFT) in the south (Chirouze, Bernet, et al., 2012; Chirouze, Dupont-Nivet, et al., 2012; Patra & Saha, 2018). In the present work, brittle structures in the Gondwana and Siwalik sequences along the Kameng River section are described and analysed. The MBT zone in the area has been studied to understand the kinematic (strain-based) and dynamic (stress-based) interpretation of the meso-scale brittle faults and joints (Angelier, 1994; Hancock, 1985; Shah et al., 2012; Simón, 2019). Here, joints are referred to as the fracture surface devoid of slip lineations (Delvaux & Sperner, 2003). As the Gondwana sequence is folded, the arrangement of joints in the meso-scale folds

**TABLE 1** The abridged stratigraphic succession of the Arunachal Himalaya along the west Kameng District, Arunachal Pradesh (modified after GSI, 2010)

Tectonic zones	Group	Formation	Lithology	Age
Sub-Himalaya	Siwalik	Kimin (Upper)	Boulder conglomerate, pebble, sandstone	Mio-Pliocene
		Subansiri (Middle)	Salt and pebble lithic arenite	Mio-Pliocene
		Dafla (Lower)	Micaceous sandstone with calcareous concretions	Miocene
<b>MBT-2</b>				
Lesser Himalaya	Gondwana Group	Bhareli	Feldspathic sandstone, siltstone, black and carbonaceous shale with thin impersistent lenticular coal	Upper Permian
		Bichom	Grey to black tuffaceous (?) shale with impersistent bands of quartzite, black shale with calcareous and phosphatic chert nodules, Diamicite with subordinate sandstone, shale, and grit.	Upper Permian
		Miri	Purple to pinkish, white to greyish, white feldspathic quartzite, purple, micaceous shale, diamicite conglomerate	Lower Palaeozoic
<b>MBT-1</b>				
	Bomdila	Bomdila Gneiss	Biotite granite gneiss	Palaeo-proterozoic
		Chilliepam	Quartzite, phyllites, schist, micaceous sandstone	
		Tenga	White to greyish-white schist, quartzite	
		Khetabari	Sericite–quartz phyllite, garnetiferous phyllite and schist	
<b>MCT</b>				

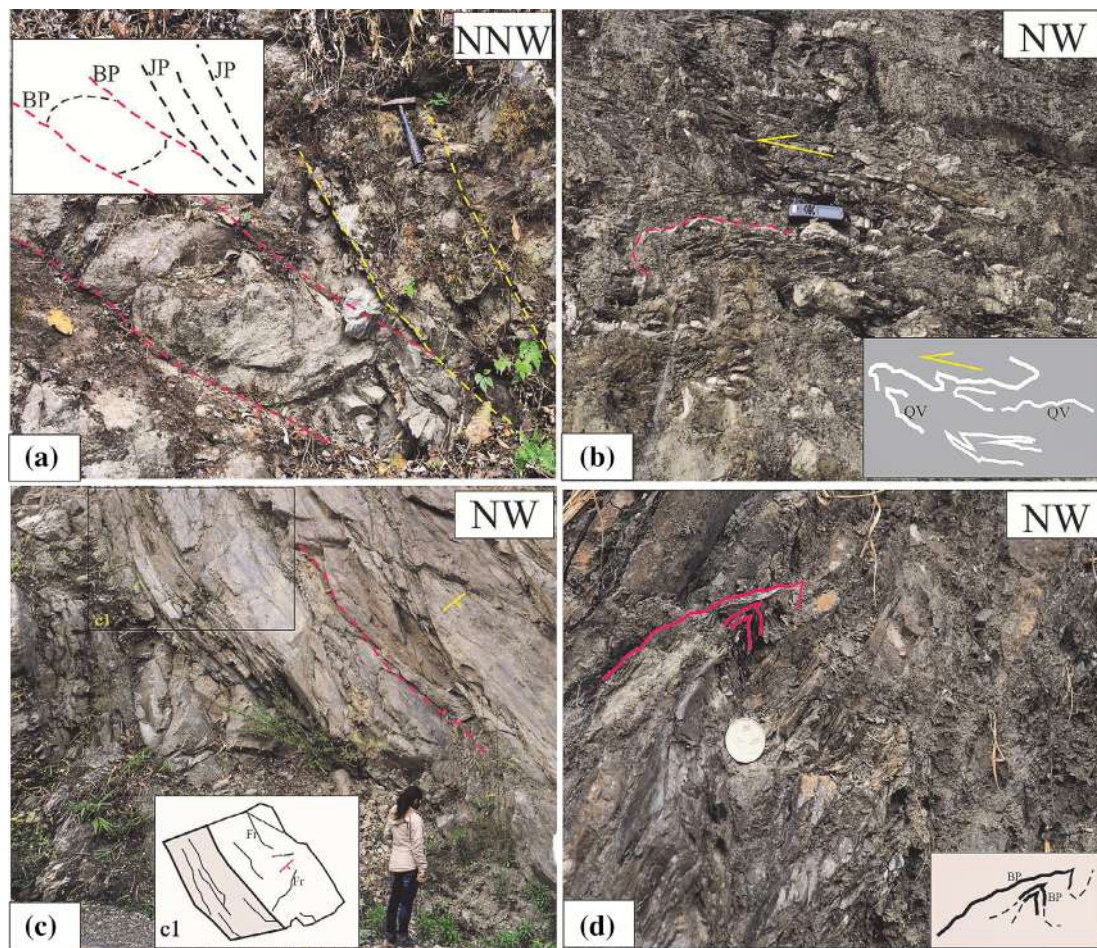


**FIGURE 3** (a) Miri Quartzite 2 km north of Sessa shows steeply dipping joint planes to the northerly direction. Red broken line: bedding in the folded Miri Quartzite (MQ). Inset-red broken line: bedding plane (BP) in MQ; broken blue lines: making an acute angle with MQ indicate joint planes (JP) in MQ. (b) Asymmetric quartz veins in MQ verge to the SE direction  $\sim 1.5$  km north of Sessa. Red broken line: folded quartz vein (QV) in MQ. Inset: bold broken white line: folded quartz vein (QV) in MQ. (c) Moderately dipping (to northerly direction) shale beds of the Bichom Formation at Sessa. Red broken line: the bedding plane. Inset: The cartoon illustrates the 3D view of the bedding plane and the orientations of the fracture on the bedding plane, shown by black lines. The attitude of the beds is shown through the red symbol. Geologist  $\sim 170$  cm height as a marker. (d) Carbonaceous shale sandstone sequence of Bhareli Formation  $\sim 1$  km north of Pinjoli. The incompetent carbonaceous shale is folded with an axis plunging  $\sim 30^\circ$  to ESE direction. Closed folds in carbonaceous shale are shown by red lines. Inset: Bedding planes (BP) in carbonaceous shale (CS) are shown by bold and black lines. BP, bedding plane; ESE, east-southeast; FR, fracture; JP, joint plane; QV, quartz vein

may also be controlled by the compositional variations in the sedimentary rocks (Winsor, 1979).

This article deduces palaeostress regime from the Pinjoli-Sessa-Nichiphu-Kimi-Bhalukpong area of western Arunachal Himalaya based on joints and faults. The study consists of outcrop mapping and field documentation of brittle structures. Finally, the palaeostress analysis is interpreted in the context of regional collisional tectonics.

## 2 | GEOLOGY

The MBT separates the Gondwana sequence from the pre-Gondwana metasedimentary sequence in the entire eastern Himalaya (Acharyya, 1980; Figure 2). Along the MBT-1, the Lesser Himalayan

Bomdila Group of rocks are thrust over the Gondwana sequence in the western Arunachal Himalaya (Singh, Singh, Sen, & Sangode, 2017). The Gondwana rocks are thrust over the Neogene Siwalik sequence along the MBT-2. The Ramgarh Thrust in the Sikkim Himalaya ( $\sim 500$  km west from the study area) underlies the Daling, Buxa, and Gondwana rocks and constitutes the Lesser Himalayan duplex (Bose & Mukherjee, 2019). In the footwall of MCT, the Ramgarh Thrust has a similar structural position in other parts of the Himalayan region such as the Kumaun-Garhwal region, Sikkim, and Arunachal Pradesh (Bhattacharyya & Ahmed, 2016; Mukherjee et al., 2015; Patel, Singh, & Lal, 2015; Pearson & DeCelles, 2005; Singh & Patel, 2017).

In Arunachal Himalaya, the Bome Thrust transports a similar Proterozoic sequence in the hanging wall with respect to the Gondwana sequence in the footwall. Four formations are included in the Permian

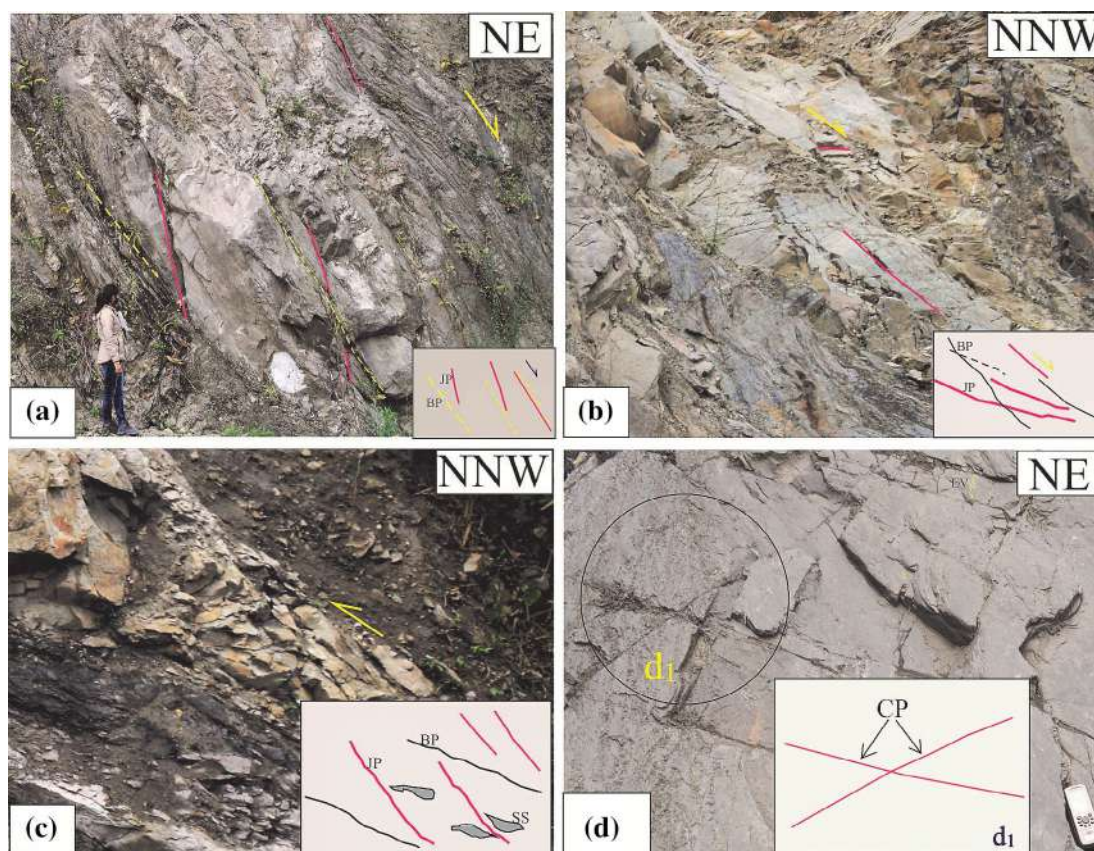


**FIGURE 4** Inclined joint sets: (a, b) ~NW-SE joint sets (J1) in the Bichom Formation ~1.5 km north of Pinjoli. (a) Geologist ~170 cm height as a marker. (c, d) ~E-W joint sets (J2) in Bhareli Formation 500 m north-east of Pinjoli. The conjugate joint sets create an X pattern with a dihedral angle of ~40°. The length of the GPS is 15.7 cm. BP, bedding plane; CP, conjugate planes; d1, magnified view of the conjugate planes; EV, extensional vein; GPS, global positioning system; JP, joint plane; SS, sigmoidal slivers

Lower Gondwana Group. Younging upward, these are the Miri, Bichom, Bhareli, and Abor volcanics (Chakrabarti, 2016; Kumar, 1997). The detrital zircon from the Miri Quartzite ~2 km north of Sessa gives the youngest age cluster as ~511 Ma. On this basis, the Miri Formation is concluded to be younger than 511 Ma (DeCelles, Carrapa, Gehrels, Chakraborty, & Ghosh, 2016). Thus, in the eastern Himalaya, the Bome Thrust (MBT-1), like the Ramgarh Thrust, can be correlated with the north Kalijhora Thrust in Darjeeling-Sikkim Himalaya and Shumar Thrust in Bhutan Himalaya (review in Bhattacharyya, Mitra, & Kwon, 2015; Mukherjee et al., 2015).

The Lesser Himalayan Sequence in the Arunachal Himalaya is well studied and has been reviewed by several workers (Bhattacharya & Nandy, 2007; Bhusan, Bindal, & Aggarwal, 1991; de Sarkar, Mathew, & Pande, 2013; DeCelles et al., 2016; Goswami, Baruah, Mahanta, Kalita, & Borah, 2020; Goswami, Bhowmik, & Dasgupta, 2009; Goswami, Bhowmik, Dasgupta, & Pant, 2014; Kumar, 1997; Ray, 1995; Ray, Bandyopadhyay, & Razdan, 1989; Saha, 2013; Sarma, Bhattacharyya, Nandy, Konwar, & Mazumdar, 2014; Singh et al., 2017; Singh & Gururajan, 2011; Singh & Singh, 1983; Srivastava, Srivastava, & Singh, 2011; Yin, 2006; Yin et al., 2006, 2010a, 2010b). However, the deformation in the Gondwana sequence within the two splays of the MBT received scanty attention.

In the Garu-Gensi area of Arunachal Pradesh, the Gondwana sequence within the Miri Thrust and MBT deformed four times (Goswami, Mahanta, Mukherjee, Syngai, & Sarmah, 2020; Mahanta, Sarmah, & Goswami, 2019; Mahanta, Syngai, Sarmah, Goswami, & Kumar, 2020). In our present area, Gondwana rocks are gently folded and brittle deformed as manifested by joints, fractures, meso-scale faults, zones of cataclasis, and fault gouges. The exposed MBT-1 at Sessa dip moderate to steeply (50–70°) to the north. In the study area, the Gondwana sequence is represented by the Lower Gondwana Miri Formation (Lower Palaeozoic) overlain by Bichom Formation (or Diuri Formation; Permo-Carboniferous) and the younger Bhareli Formation (Permo-Carboniferous; GSI, 2010; Table 1). In the eastern part, along the Pinjoli-Nichiphu-Kimi traverse, the rocks of the Bhareli Formation exhibit a northwest-southeast (NW-SE) trending strike-slip zone of ~20 m thickness and ~10 m offset to the SE direction.

The contact between Bhareli and Bichom formations is gradational. Therefore, we consider that both the Bhareli and the Bichom formations were thrust along the MBT-2 as a single unit maintaining their internal stratigraphy. The white to greyish-white Miri Quartzite dips ~65° northerly and is interlayered with silty shale and phyllite (Figure 3a). The Miri Quartzites along MBT-1 are intensely deformed and mylonitized. Shear-related folded quartz veins in the Miri

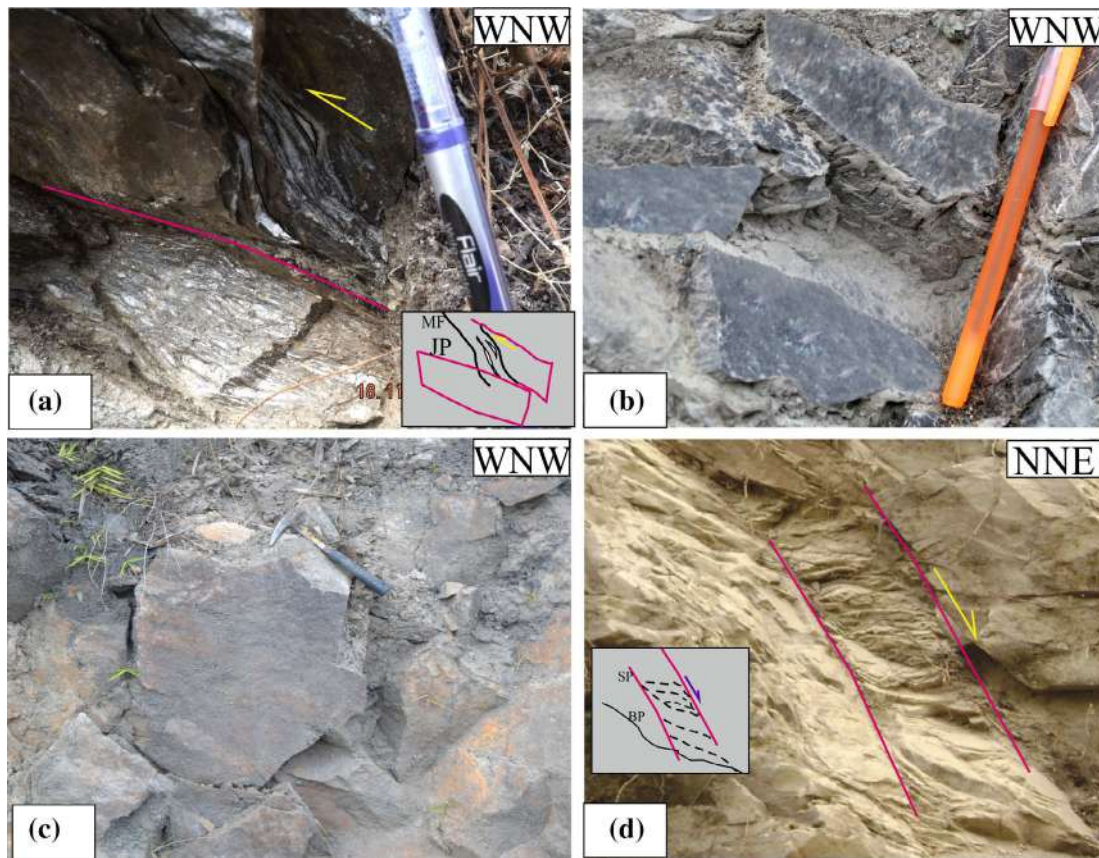


**FIGURE 5** Subvertical joint sets. (a) WNW trending subvertical joints in Bomdila Gneiss ~3 km north of Sessa. The length of the pen is 14 cm. (b, c) ~WNW trending joint planes in Miri Quartzite ~1.5 km north of Sessa. Length of the pen: 13 cm. (d) ~ESE trending subvertical shear plane in Dafla Sandstone near Kamla River-bridge ~1 km south of Pinjoli. BP, bedding plane; JP, joint plane; MF, Mylonitic foliation; SP, shear plane; WNW, west-northwest

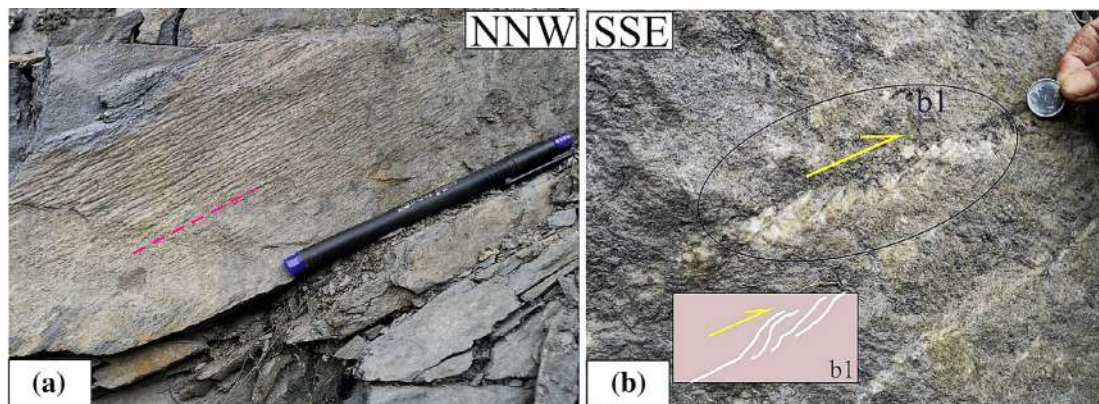


**FIGURE 6** Strike-slip fault zone: (a) Subhorizontal striae in the Bhareli Sandstone ~2 km ENE from Pinjoli. The pitch is ~15° from the south. (b) En-echelon veins in the Bhareli Sandstone from the same area indicate NW-directed sense of shear. (b1): the magnified view of the en-echelon veins. The continuity of the fault zone to the Siwalik sequence could not be studied due to inaccessible terrain

Quartzite trend east-northeast (ENE) with south-southwest (SSE)-vergence (Figure 3b). The Miri Quartzites are stratigraphically overlain by the rocks of the Bichom Formation with a unit of diamictite at its base. The Bichom Formation consists of grey to black shales with

alternating sand layers (Table 1 and Figure 3c). The shale sand layer dip moderately to a northerly direction along the Pinjoli-Sessa traverse (Figure 3c). The Bhareli Formation consists of alternating layers of greyish coloured medium- to coarse-grained sandstone and

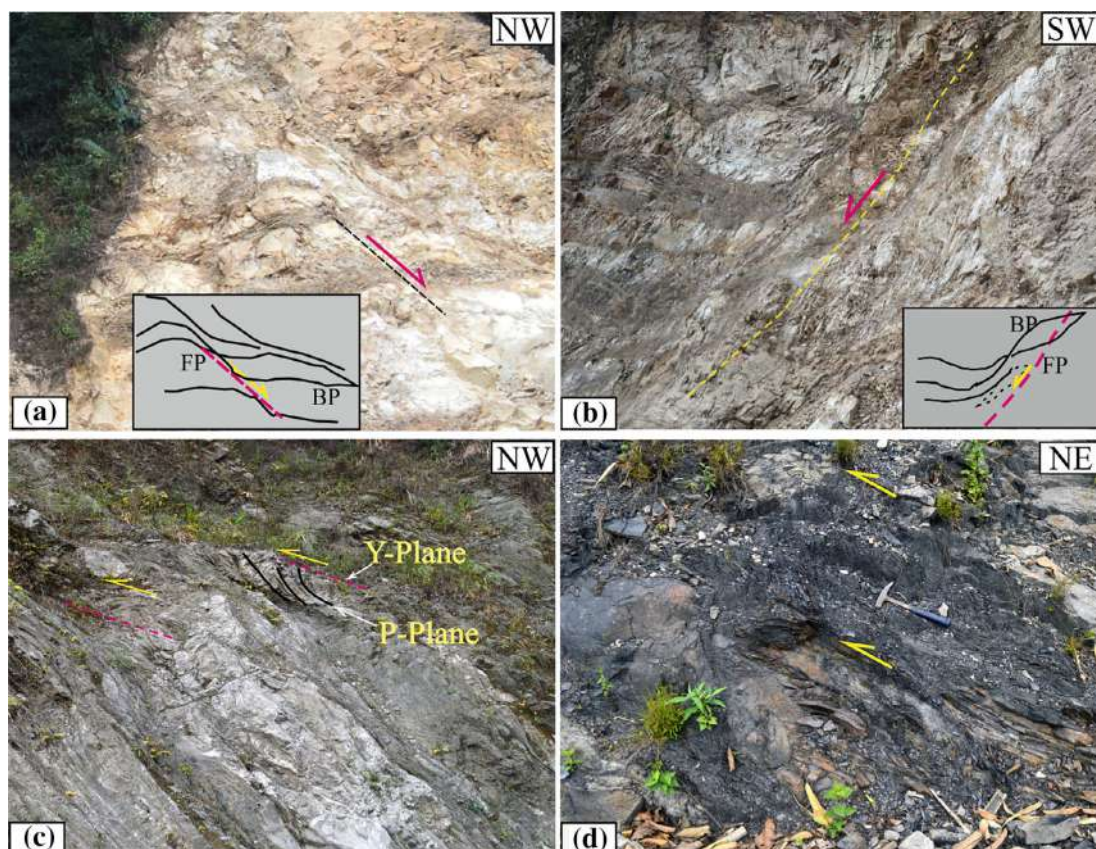


**FIGURE 7** (a, b): top-to-NW down and top-to-NE down normal sense of slip in the Miri Quartzites in the ~2 km north of Sessa. (c) Top-to-SE up slip sense in the Bichom Formation in the ~500 m north of Sessa. The P-planes are pointing to the directions of movement and curved at one place (d) top-to-SW up sense of slip in the sandstone carbonaceous shale sequence of the Bhareli Formation in the north of Pinjoli. The incompetent carbonaceous shale bed is folded and asymmetry is towards the direction of slip. BP: bedding plane; FP: fault plane; NE, northeast; NW, northwest

carbonaceous shale with patchy occurrences of coal beds. Tightly folded carbonaceous shales are documented along the Pinjoli-Sessa and Pinjoli-Nichiphu-Kimi traverse (Figure 3d). The rocks of the Bichom and Bhareli formations together exhibit a ramp and flat geometry and constitute a thickness of ~5 km in the study area (DeCelles et al., 2016; Yin et al., 2010b). The dip of the beds near MBT-2 increases up to ~70° and near Kimi, the dip decrease to 55–60°. The rocks of the Lower Siwalik Dafla Formation near MBT-2 exhibit a steep dip (~75°) and the dip decrease southward gradually (Goswami, Bezbaruah, Mukherjee, Sarmah, & Jabeed, 2018). Meso-scale fractures from the Bomdila Group, the Gondwana Group, and Lower and Middle Siwalik Dafla and Subansiri formations are considered in this study for palaeostress analysis.

### 3 | FIELD DOCUMENTATION

The present area was mapped by the Geological Survey of India in the 1980s and 1990s which are accessed from the Bhukosh database, Geological Survey of India (GSI). We have prepared an updated geological map from the data gathered from the present mapping

traverse that connects townships of Bhalukpong, Pinjoli, Sessa, Nichiphu, and Kimi in the western Arunachal Pradesh. Mapping was done on the toposheet nos. 83A/8 and 83A/12 at 1:50000 scale. Brittle deformation of rocks was undertaken along three traverses: Traverse 1: From Pinjoli Nala to ~2 km north of Sessa covering a distance of 7 km; Traverse 2: From Pinjoli through Nichiphu to Kimi village (distance: ~15 km) and Traverse 3: from north of Bhalukpong to Pinjoli (distance: 13 km). These traverses together cover ~120 km<sup>2</sup> in the west Kameng District of Arunachal Pradesh (Figure 2). Brittle tectonics manifested by joints is classified as (a) inclined joints, (b) conjugate shear joints, and (c) subvertical joints. We also documented meso-scale faults, en-echelon veins, and disharmonic folds.

#### 3.1 | Joints

Both planar and curvilinear joint surfaces are observed in the area. Four joint sets are documented. Two sets of subvertical joints are recorded from the Miri Formation (Gondwana Group) in the footwall of MBT-1 and the Dafla Formation (Lower Siwalik Group) in the

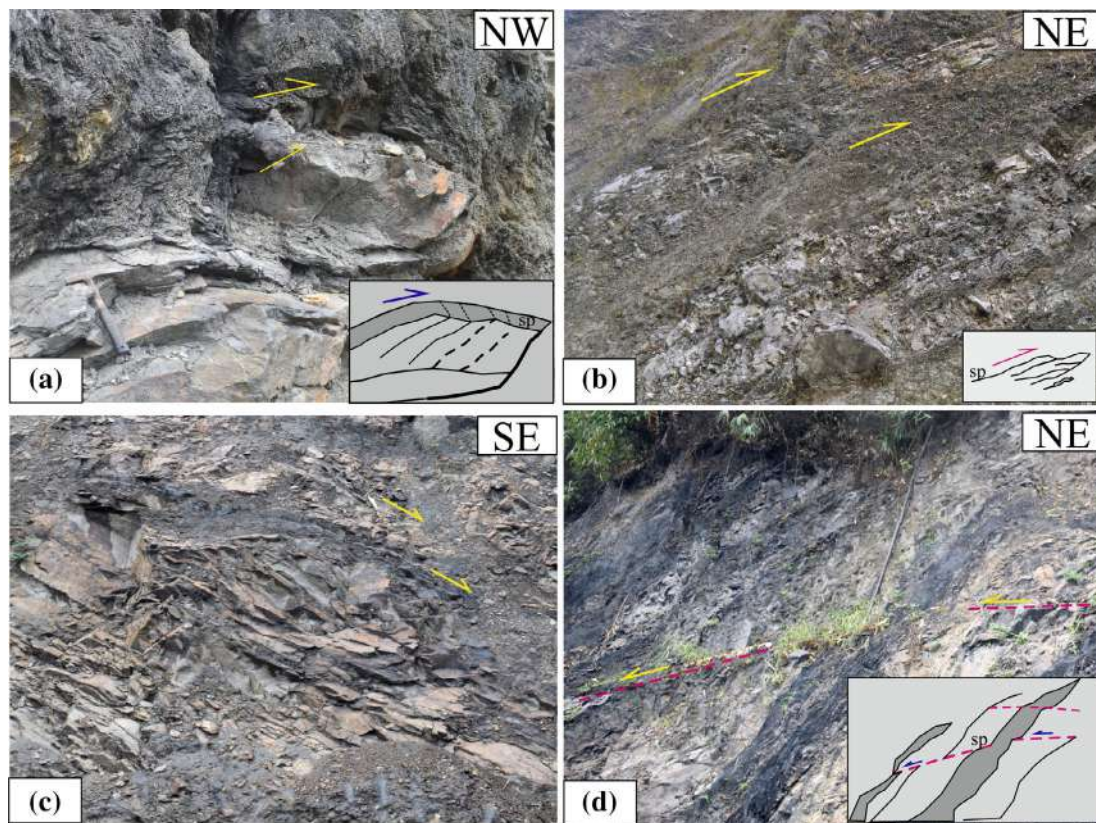


**FIGURE 8** (a) Top-to-NW up sense of slip in the sandstones of the Bhareli Formation in the north of Pinjoli. Y and P-planes in the middle are forming a duplex-type structure. The hammer is 28 cm in length. (b) Top-to-NE sense of slip in the Bichom Formation in the north of Sessa. (c, d) top-to-SE down and top-to-SW down sense of shear in the sandstone carbonaceous shale sequence of the Bhareli Formation in the ~200 m north of Pinjoli; this sense of shear is difficult to interpret—see text for details. NE, northeast; SE, southeast; SP, shear plane; SW, southwest

footwall of MBT-2. Inclined joint sets are documented from the Bichom and Bhareli formations of Gondwana rocks in the hanging wall of MBT-2. The joint plane locations are shown in Figure 2. Two sets of inclined joints are (a) NW-SE (J1) (Figure 4a,b), (b) ~EW (J2) (Figure 4c,d—conjugate planes included); and two sets of subvertical joints are (c) west-northwest-east-southeast (~WNW-ESE, J3) (Figure 5a,b), and (d) ~NNE-SSW (J4) (Figure 5c,d). The J2 joint sets include conjugate joint sets. Dips of the joint planes in the inclined joint sets (J1 and J2) are  $\leq 60^\circ$  and for the subvertical joint sets, it is  $\geq 80^\circ$ . Conjugate joints (J2) in the field are associated with dilational veins (Figure 4d). Geometries of joints may be correlated to their geneses. The unidirectional joint system generally displays an I-shape pattern (Hancock, 1985). The dihedral angle ( $2\theta$ ) of the conjugate hybrid joint is found to vary between  $35$  and  $45^\circ$  (Hancock, 1985). In the present study, the value of  $2\theta$  is found to be within the range ( $\sim 40^\circ$ ). The association of orthogonal joints with the conjugate shear joints indicates changing shearing strength of the rocks. High shear strength may initially allow the formation of conjugate joint sets followed by orthogonal joints during the layer normal compression (Mandl, 2005). Further, the dihedral angle between the two conjugate shear planes depends on the differential stress and the angle of internal friction of the rocks (Simón, Arlegui, Liesa, & Maestro, 1999). In the present study, we have characterized some of the conjugate J2 joints as the conjugate shear joints (Figure 4d).

### 3.2 | Strike-slip zone

About 5 km ENE of Pinjoli, we documented a fault zone in the sandstone-shale unit of the Bhareli Formation with subhorizontal fault strain with  $\sim 15^\circ$  pitch to SSE on a subvertical fault plane. Further, the en-echelon quartz veins depict an SSE-directed shear (Figures 6a,b). The fault zone is  $\sim 20$  m thick with  $\sim 10$  m offset. However, the continuation of the strike-slip zone through the Siwalik could not be studied because of the inaccessibility of the terrain. Therefore, we could not include the strike-slip data in the palaeostress analysis.

### 3.3 | Mesoscopic faults

Faulting in sandstones exhibits various shear senses. Eight different mesoscopic faults with sense of shear are documented in the field: (a) top-to-NW (up) (F1), (b) top-to-NE (up) (F2), (c) top-to-SE (down) (F3), (d) top-to-NE (down) (F4), (e) top-to-SW (down) (F5), (f) top-to-SW (up) (F6), (g) top-to-SE (up) (F7), and (h) top-to-NW (down) (F8). The data pertaining to ENE-trending near-vertical faults are listed in the supplementary tables. We have utilized the different markers to ascertain the slip senses: (a) *Displacement of the markers*: Incompetent beds of carbonaceous shale and grey shale alternating in sandstone layers (Figures 7d and 8c,d; as per Liang, Peng, Du, & Lu, 2018;

Morely, 2017), (b) *Y and P-brittle shear planes*: Y and P planes are found in many brittle fault zones (Figure 7c). The P-planes characteristically merge with the Y-planes tangentially (Chen et al., 2014; Doblas, 1998; Mukherjee & Chakraborty, 2020). The Y-shears act as a boundary fault for the brittle fault zone or are parallel to the boundary of the fault (Passchier & Trouw, 2005). The angle between the Y-planes and the P-planes vary between 20 and 50° (Davis, Reynolds, & Kluth, 2012; Passchier & Trouw, 2005), whereas in the present study, the estimated angle varies between 30 and 50°. It is noteworthy that the en-echelon inclined P-planes are commonly inclined towards the movement of the opposite block (Doblas, 1998). Brittle slips are convincingly determined from the Y- and P-planes in many brittle fault zones in the Himalaya (Mukherjee & Koyi, 2010a, 2010b) and elsewhere (Passchier & Trouw, 2005). The angular relationship of the Y- and P-planes helped us to determine the sense of shear. (c) *Asymmetric folds*: These are also utilized to decipher the sense of

shear in the field (Mukherjee et al., 2015, 2019). Many of these folds are rootless and disharmonic type and verge invariably towards the foreland locally defining forefolds (Figure 3b). (d) *En-echelon veins*: These are utilized to determine the shear sense in the study area (Figure 6b; Passchier & Trouw, 2005).

The first phase of brittle deformation under NNW-directed extension is manifested by subvertical joint planes in the Proterozoic Bomdila Gneiss (Figure 5a). Top-to-NW down and Top-to-NE down normal senses of displacement is observed in the Miri Formation in the footwall of MBT-1 (Figures 7a,b). The Miri Formation is the oldest unit of the Gondwana sequence and therefore the pre-Himalayan extension phase is imprinted in the Miri rocks before the Mio-Pliocene Himalayan Orogeny. The compressional phases of Himalayan orogeny are documented in the Bichom and Bhareli formations in the hanging wall of MBT-2. The compression phases are recorded in four senses of fault slip: top-to-SE up (Figure 7c) and top-to-NE up

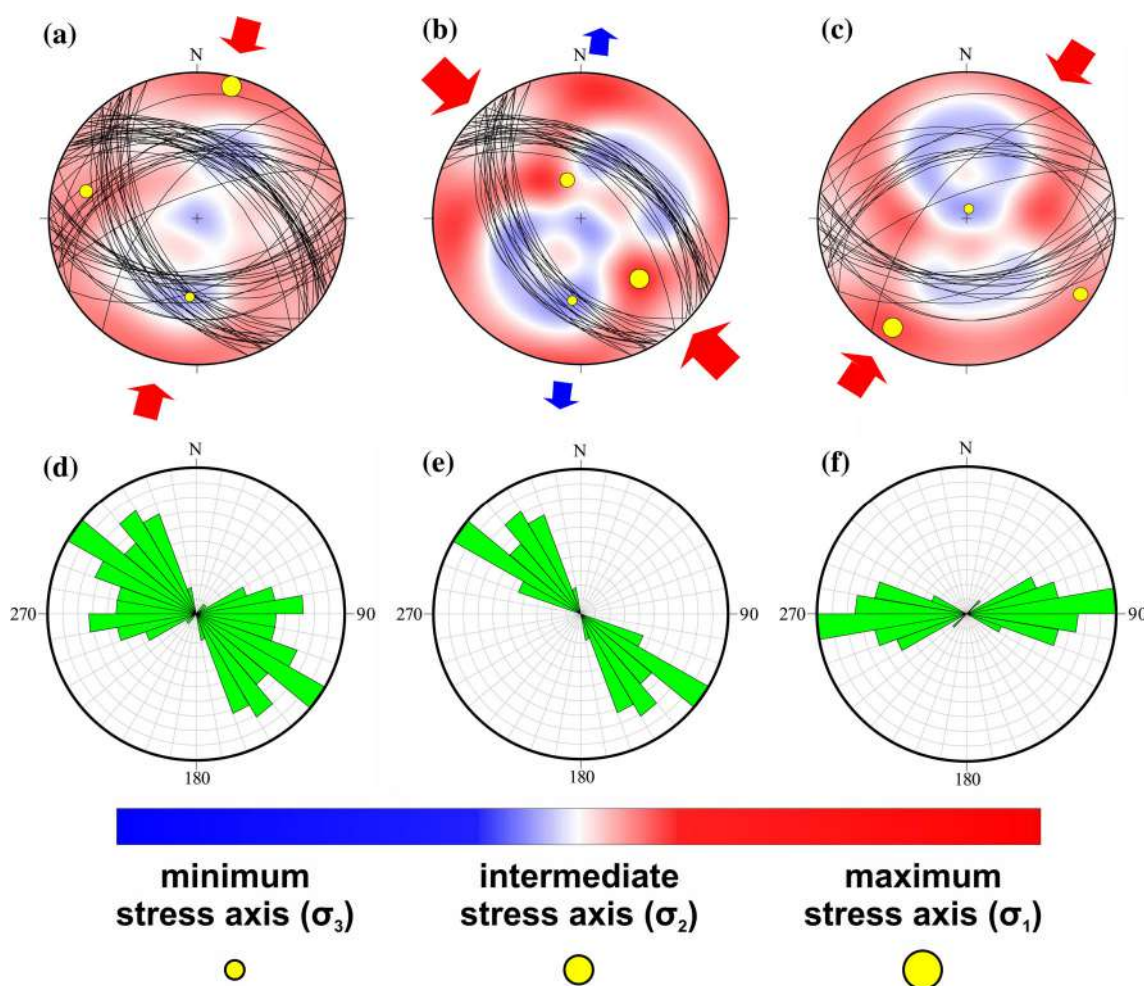


**FIGURE 9** Palaeostress analysis results generated by using visualization of the Gauss function (VGF) implemented in T-Tecto studio X5 (Žalohar & Vrabec, 2007). (a–c) Lower hemisphere equal-area projections of all inclined joints (J1 and J2;  $n = 73$ ;  $n$ : number of joints used in the analysis), ~NW-striking J1 set ( $n = 42$ ) and ~W-striking J2 set ( $n = 31$ ), respectively. Black lines: attitude of joint planes. Red and blue quadrants (also represented in the horizontal scale bar below): regions of compression and tension, respectively. Biggest, medium, and smallest yellow circle symbols: orientation of maximum ( $\sigma_1$ ), intermediate ( $\sigma_2$ ), and minimum ( $\sigma_3$ ) stress axes, respectively ( $\sigma_1 \geq \sigma_2 \geq \sigma_3$ ). Red inward-pointed and blue outward-pointed double arrows at the periphery of the stereoplots: orientation of maximum ( $S_{Hmax}$ ) and minimum ( $S_{Hmin}$ ) horizontal stress, respectively. (d–f) rose plots for orientations of all inclined joints, J1 set and J2 set, respectively

(Figure 8b) in the Bichom Formation; and top-to-SW up (Figure 7d) and top-to-NW up (Figure 8a) in the Bhareli Formation. Two other slip senses: top-to-SE down (Figure 8c) and top-to-SW down (Figure 8d) noted in the Bhareli Formation are difficult to interpret and may be related to the orogen-parallel ~E-W extension phase of the Siwalik sequence in the phase 3 extension (Section 6). Orogen-parallel shear has recently been discussed from sub-Himalaya in Dutta et al. (2019) and from the Lesser Himalaya in Mahato, Mukherjee, and Bose (2019) and Biswas, Bose, Dutta, and Mukherjee (2022), all from the western Himalayan sector. It is significant to note only a few places fault striae are documented. The slip data indicate a normal sense of shear contrary to the reverse sense in some places as mentioned and the curvilinear nature of the fault plane as well.

#### 4 | PALAEOSTRESS ANALYSIS

The fault-slip data are documented from a terrain consisting of multiple slip directions. The palaeostress analysis is utilized to determine the stress tensors that justify these multiple slips. Through the fundamental works by Anderson (1905, 1951), the

relationship between the fault and stresses in the crust was well presented. The numerical approach of this relationship can be explained through the Wallace–Bott hypothesis, which states that the slip on the fault plane takes place parallel to the direction of maximum resolved shear stress (Bott, 1959; Wallace, 1951). The orientation of the fault plane must be as per the Mohr–Coulomb yield criterion or the shear to the normal stress ratio is equal to  $\tan \phi$ , where “ $\phi$ ” is the angle of internal friction (Coulomb, 1776). Based on these criteria, we can estimate the stresses for reactivation of crustal faults and the process is called the stress inversion method. It derives reduced stress tensor from the field-acquired fault slip data (e.g., Angelier, 1984, 1989, 1994; Delvaux & Sperner, 2003; Marrett & Allmendinger, 1990; Tranos, 2015, 2018). Several methods are in use for analysing palaeostress (Simón, 2019). Some techniques use the geometrical and others use the frictional criteria and still, there are a few techniques that combine both geometrical and frictional criteria (Célérier, 1988; Žalohar & Vrabec, 2008). It is noteworthy that faults are activated when the resolved shear stress exceeds the frictional resistance of sliding according to Amantons Law of Friction and stresses that induce slip are homogeneous regionally (e.g., Nemcok & Lisle, 1995; Twiss & Unruh, 1998; Yamaji, Otsubo, &

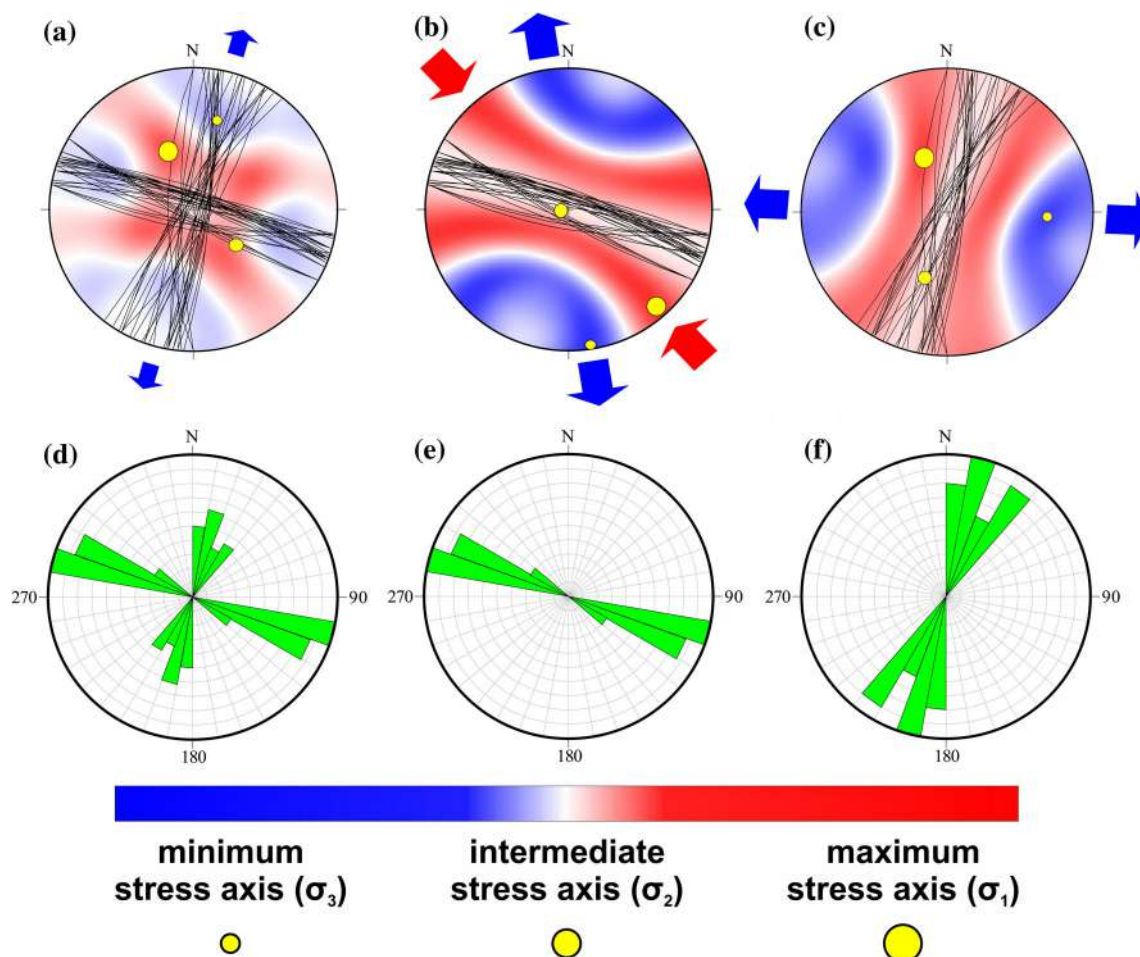


**FIGURE 10** (a–c) as for Figure 9 (a–c) but for all subvertical joints ( $n = 68$ ) in (a), ~WNW-striking J3 set ( $n = 35$ ) in (b) and ~SSW-striking J4 set ( $n = 33$ ) in (c). (d–f) rose plots for orientations of all near-vertical joints, J3 set and J4 set, respectively

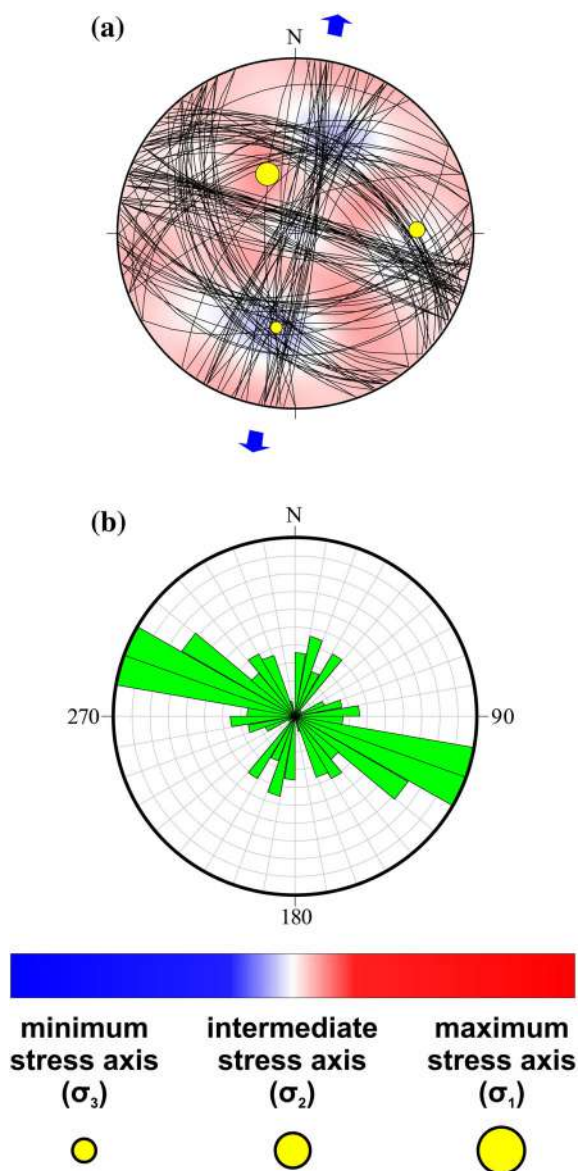


**FIGURE 11** (a, b) Palaeostress tensor and rose plot for all inclined and subvertical joints ( $n = 141$ ), respectively. Same as Figure 9 caption for interpretation of palaeostress tensor deduced by T-Tecto studio X5 (Žalohar & Vrabec, 2007)

Sato, 2006; Zolohar & Vrabec, 2010). Information on the relative attitude of faults and attitudes of net-slip helps us to determine the magnitudes and orientations of the principal stresses. Thus, the orientations of the three principal stress axes at the time of faulting can be calculated through the palaeostress analysis.

We have used T-TECTO Studio X5 (developed by Zolohar, 2015) to analyse the palaeostress. We use the notion that compression is positive with  $\sigma_1 \geq \sigma_2 \geq \sigma_3$  and stress ratio  $R = (\sigma_2 - \sigma_3)/(\sigma_1 - \sigma_3)$  in our calculations (Spener & Zweigel, 2010). Here,  $\sigma_1$ ,  $\sigma_2$ , and  $\sigma_3$  are the maximum, intermediate, and minimum compressive principal stress axes, respectively, and are conventionally considered as positive (Twiss and Moores, 2007). Significantly, the slip direction (parallel to the shear stress) along the fault plane depends on the orientations

of these stress axes. Further, the slip direction also depends on the magnitudes of the  $\sigma_1$ ,  $\sigma_2$ , and  $\sigma_3$ . Thus, the shape of the stress ellipsoid is described by the ratio  $R$  and the  $R$ -value varies between 0 and 1.  $R = 0$  indicates a prolate uniaxial compressional ellipsoid ( $\sigma_1 > \sigma_2 = \sigma_3$ ).  $R = 1$  connotes oblate uniaxial extensional ellipsoid ( $\sigma_1 = \sigma_2 > \sigma_3$ ; Delvaux et al., 1997).

To perform the analysis, the program requires the type of joints, their azimuth, and dip direction parameters to be entered. The joint plane's data were divided into inclined and subvertical sets, which were further subdivided into four joint sets: (a) ~NW-striking inclined J1 set, (b) ~W-striking inclined J2 set, (c) ~WNW-striking subvertical J3 set, and (d) ~SSW-striking subvertical J4 set. Individually, all four joint sets were examined, followed by inclined joints (J1 and J2 together) and subvertical joints (J3 and J4 together). All 141 joints were also evaluated in a separate run to deduce the palaeostress tensor.

The T-TECTO Studio X5 uses the Right Dihedra Method (RDM; Angelier & Mechler, 1977). The RDM advocates that the maximum principal axis is constrained to the pressure (P) quadrant and the minimum principal stress axis to the tension/extension (T) quadrant of a selected fault. On the other hand, the Visualization of the Gauss object Function (VGF) of Žalohar and Vrabec (2007) estimates the areas of the high probability of maximum and minimum principal stress orientations (Žalohar & Vrabec, 2007). VGF method helps to obtain the analysis of various joints and faults. The VGF calculates the optimum probable orientations of maximum ( $\sigma_1$ ) and minimum ( $\sigma_3$ ) principal stresses for a group of faults under the condition of common stress. Various RDM methods help analyse the faults and accordingly the orientations of the principal stress axes are determined.

## 5 | DATA AND METHODS

Brittle deformation is most commonly manifested by the development of mesoscale joints. The dynamic palaeostress analysis of such brittle structures is critical for determining the regional palaeostress conditions that exist in the study area (e.g., Dutta et al., 2019; Maurya, Shaikh, & Mukherjee, 2021; Shaikh et al., 2020; Vanik, Shaikh, Mukherjee, Maurya, & Chamyal, 2018). We investigate palaeostress conditions using structural data consisting of 141 joint planes collected in the field (Figure 2). Among the 141 joint planes, there are 73 inclined and 68 subvertical varieties. We have also recorded attitudes and slip senses of various mesoscale faults from the area (Pinjoli-Sessa, and Pinjoli-Nichiphu-Kimi).

From these data sets, we analysed the palaeostress using T-TECTO Studio. Note (a) for tension or extension fractures (T or E), the maximum compression axis  $\sigma_1$  lies in the fracture plane and the minimum compression axis  $\sigma_3$  is perpendicular to the fractures. (b) For shear fractures, the  $\sigma_1$  axis lies oblique to the fractures plane and  $\sigma_3$  is perpendicular to the  $\sigma_1$ . For the conjugate shear fractures, the angle between the  $\sigma_1$  and the fracture plane ranges ~15–20°. This conforms with the variation of the dihedral angle  $2\theta$  (~35–45°). It is supposed

**TABLE 2** Joint data sets in different formations in the Gondwana and Siwalik sequences, western Arunachal Himalaya as plotted in Figure 2

Symbol	Locations/site	Formation	Nature of joints	Number of joint data	Total number of sets
Solid circle blue	M 111	Miri quartzite	Subvertical	11	35
	M 113	Miri quartzite	Subvertical	09	
	M 114	Miri quartzite	Subvertical	07	
	M 121	Miri quartzite	Subvertical	06	
	M 127	Miri quartzite	Subvertical	04	
Solid circle yellow	B-024	Bhareli	Inclined	10	42
	B-028	Bhareli	Inclined	06	
	B-031	Bhareli	Inclined	06	
	B-051	Bhareli	Inclined	07	
	B-056	Bhareli	Inclined	05	
	B-061	Bhareli	Inclined	03	
	B-076	Bhareli	Inclined	02	
	B-078	Bhareli	Inclined	03	
Solid circle green	Bi 081	Bichom	Inclined	09	31
	Bi 086	Bichom	Inclined	06	
	Bi 097	Bichom	Inclined	07	
	Bi 098	Bichom	Inclined	03	
	Bi 101	Bichom	Inclined	06	
Solid circle red	D 131	Dafla	Subvertical	11	33
	D 134	Dafla	Subvertical	05	
	D 137	Dafla	Subvertical	06	
	S 139	Subansiri	Subvertical	08	
	S 140	Subansiri	Subvertical	03	

that the fractures formed at the same tectonic phase have the common intersection of the compression and tension areas. In the present study, initially, we have analysed all the joint sets individually for the rocks of the Bhareli, Bichom, Dafla, and Bomdila Gneisses for ascertaining the palaeostress directions.

## 6 | RESULTS

The results of the palaeostress analysis are shown in Figures 9–11. The stress ratio cannot be determined from the T-TECTO Studio X5 solely from fracture data. The present algorithm of the software can determine the stress ratio only when the fault slip data are utilized (Dutta et al., 2019).

We have recorded measurements of 141 joint sets in the Lower Gondwana Miri, Bichom, and Bhareli formations and Lower Siwalik Dafla Formation in the present study. Table 2 presents the joint set data. Data subsets in each site are shown in Figure 2. Each data subsets are given an alphabetical prefix corresponding to each stratigraphic unit: M for the Miri Formation, Bi for Bichom, B for Bhareli Formation discriminated by different numeric codes as a suffix, D for Lower Siwalik Dafla Formation, and S for Middle Siwalik Subansiri Formation (Figure 2). On the basis of the results of the palaeostress analysis performed for the nature of the

individual set of joint data, we have interpreted the chronology of the brittle deformation in the present area.

### 6.1 | Phase 1: Pre-Himalayan extension recorded in the Miri Formation

The WNW-striking subvertical joint sets (J3;  $n = 35$ ) in the rocks of the Miri Formation in the hanging wall of MBT-2 depicts a ~NNW-directed extension (Figure 10b). However, the palaeostress analysis yields a subhorizontal  $\sigma_1$  and  $\sigma_3$  and ~vertical  $\sigma_2$  for this joint set. Note WNW-NW-oriented inclined and subvertical joints are developed under ~NW-oriented compression and ~NNW-NNE-oriented extension. The NNW-oriented extension is consistent with the pre-Himalayan stress regime deduced for Lower Gondwana rocks of the Darjeeling-Sikkim Himalaya (Patra & Saha, 2018).

### 6.2 | Phase 2: Himalayan compression recorded in the Bichom and Bhareli formations

Two inclined sets of joints were recorded in the Bichom (J1) and Bhareli (J2) formations in the hanging wall of MBT 2 (Table 3). These

**TABLE 3** Results of the palaeostress analysis

	Orientation of the principal stress axis			
	Trend/plunge (°)			
	$\sigma_1$	$\sigma_2$	$\sigma_3$	
<b>Joints</b>				
Inclined (Figure 11)	All	14/2	284/13	186/32
	J1	136/29	341/58	186/30
	J2	241/05	124/03	11/82
Near vertical (Figure 12)	All	337/41	130/46	15/22
	J3	138/03	262/84	171/00
	J4	337/44	198/37	93/19
Both inclined and near vertical (Figure 11)		334/48	88/20	191/31

two sets of joints in the footwall of the MBT-1 yield near-horizontal  $\sigma_1$  (Table 3). The ~NE-oriented compression with horizontal  $\sigma_1$  is revealed by the inclined joint sets (J1 and J2=; ( $n = 73$ ) development when considered together (Figure 9a). When ~W-striking J2 set ( $n = 31$ ) is analysed alone, the result seems to be the same with horizontal  $\sigma_1$  and  $\sigma_2$ ; and vertical  $\sigma_3$  (Figure 9c). When only ~NW-striking J1 set ( $n = 42$ ) is taken into account, the ~NNE-oriented extension and ~NW-oriented compression come out. The ~NW-oriented compression bisects the acute angle between the conjugate joint sets (Figure 9b).

### 6.3 | Phase 3: E-W extension in the Lower Siwalik Dafla and Middle Siwalik Subansiri formations

The subvertical ~SSW-striking J4 set ( $n = 33$ ) recorded in the Dafla and Subansiri formations are analysed together, and ~W—the directed extension is revealed (Figure 10c). Palaeostress analysis, however, yields a moderately inclined  $\sigma_1$  and low to moderately inclined  $\sigma_2$  and  $\sigma_3$  axis (Table 3).

In the present investigation, we could not record any strike-slip stress regime from the area on the basis of fracture data or fault striae. However, along the Pinjoili-Nichiphu-Kimi traverse we have recorded en-echelon veins indicating top-to-NW shear (Figure 6). Further, two planes exhibiting subhorizontal striae may indicate strike-slip offset in the MBT. Accordingly, we have shown this zone as ~NW-SE striking strike-slip zone on the map (Figure 2).

Therefore, two prominent orientations of compression—NW and NE, two prominent orientations of extension—NNW-NNE and ~W are deduced, which are responsible for the generation of inclined and subvertical joint sets of the present area. When all the inclined and near-vertical joints are analysed together ( $n = 141$ ; Figure 11), ~NNE-oriented extension is observed, which resembles the result obtained in Figure 10a.

## 7 | DISCUSSION

Reconstruction of the palaeostress in the Gondwana sequence of the study area helps us to understand the stress regimes that might have prevailed during the evolutionary history of different stratigraphic units. The Gondwana sequence is folded and there is little information on the nature and attitude of the fracture surfaces in different lithotectonic units of the area. De Sarkar et al. (2013) studied the lineament trends in the stratigraphic units of the Gondwana, Bomdila, and Sela Group of rocks. Accordingly, the lineaments are classified based on their trends as WNW-ESE, NW-SE, NNW-SSE, N-S, NNE-SSW, NE-SW, and ENE-WSW. The arc-parallel extension has been reported from the western Arunachal Himalaya (De Sarkar et al., 2013). The E-W extension is manifested through arc perpendicular extension faults and arc parallel strike-slip faults in the hinterland (De Sarkar et al., 2013).

Observations on the fractures planes and mesoscopic faults across the MBT zone in the Gondwana and Lower Siwalik Dafla sequences are documented in this study. We have also recorded eight mesoscopic faults with slip senses. These faults may indicate the phases of compression during the Miocene Himalayan orogenesis. However, shear senses indicating normal (top-to-SW down) and reverse movements (top-to-SE up) are difficult to interpret. These senses may indicate local or regional changes in the stress regimes. Well-defined fracture planes are recorded from the Gondwana, Dafla, and Bomdila Gneisses. Note that joints and faults cannot be regarded as kinematic equivalents, but under similarly oriented stress fields, both structures can form (Roberts, 1975). Prefaulting damage may be initiated with pervasive fracturing. In general, the faulting episodes are preceded by fracture development, and fracturing decreases with the increasing distance from the fault. Further, faulting may be formed on earlier formed joints (Mandl, 2005). Steeply dipping faults may develop conjugate fracture planes. The ENE-WSW trending inclined joints (J2) indicate a NE-SW directed compression as evidenced by the trend of the axis of the antiforms in the Gondwana sequence at some locations (Figure 2). The ~E-W subvertical joint sets are also nearly parallel to the trend of the MBT and axis of folded Gondwana and Dafla sequence in the area (Figure 2). All joint sets and faults are not coeval and require the maximum compressive stress to be oriented subparallel to the trend of the bedding and intermediate compressive axis perpendicular to the bedding (Roberts, 1975). Near-vertical faults in the Siwalik sequence of the western Himalaya can be related to isostatic adjustments and strike-slip tectonics. Dutta et al. (2019) provided a similar interpretation from the western sub-Himalaya.

From the present study, two prominent orientations of compression—NW and NE, two prominent orientations of extension—NNW-NNE and ~W are deduced, which are responsible for the generation of inclined and subvertical joint sets. We have analysed the inclined and subvertical joints together (Figure 11). It is observed that the result is similar to Figure 10a where all subvertical joints are considered together. The NNE-oriented extension is difficult to explain and may indicate a pre-Himalayan phase along with the NNW-

directed extension. However, also note that the absence of inward-pointing double arrows in Figure 11a indicates that the program was unable to determine the dominant compression direction when all joint data of different orientations were run together. Note that combining all of the joint sets in a single run implies that we agree that all of the joint sets (conjugate/systematic/nonsystematic) were generated at the same time. As a result, we are ignoring their relative timing of formation and therefore coeval genesis sounds unlikely.

In the present study, the joint plane orientations covered an area of 120 sq km in two traverses along with N-S and NE-SW directions across MBT-1 and MBT-2. Three phases of brittle deformation indicating three stress regimes in the area have most explicitly emerged from this study.

The Miri Formation in the footwall of MBT-1 represented the NNW-directed extension along with the NW-directed compression. The extension phase is pre-Himalayan and related to the Early Permian tensional phases of the Gondwanan Indian shield where deposition Miri Formation sediments were taking place. Eventually, the Miri sediments suffered further extension in the subsequent rift phases (Biswas, 1999; Mahanta et al., 2021; Wopfner & Jin, 2009). Therefore, the pre-Himalayan brittle extension in the Lower Gondwana rocks represents an inherited brittle deformation. Subsequently, during the Miocene Himalayan Orogeny, these inherited brittle deformation features are intersected by the MBT-1.

The features of the second phase of brittle deformation in the area recorded in the Bichom and Bhareli formations indicate Himalayan orogenesis. The data sets covering both the formations indicate the NNE-SSW-directed compression and the principal stress axis vary

orientation from NW to NE directions. The low plunge of the  $\sigma_1$  is observed in the inclined data sets (Figures 9a–c). However, the apparent flip of  $\sigma_2$  and  $\sigma_3$  is observed. This may be due to continued thrusting and thrust loading made  $\sigma_2$  subvertical (Fossen, 2016).

The ~E-W extension recorded in the Siwalik sequence represents orogen-parallel extension in the outer arc of the fold-thrust belt in the Kameng River section of the Arunachal Himalaya. Joint data sets from the Lower and Middle Siwalik Dafla and Subansiri formations might have formed during the thrust transportation of the Gondwana sequence over the Siwalik sequence along MBT-2. The extension might also take place during thrusting of the Lower Siwalik over the Subansiri rocks along the Tipi Thrust. Thus, the orogen parallel extension is documented in the foothills of the western Arunachal Himalaya. In this context, the result of the present study is consistent with the ~E-W extension reported in the Siwalik sequence of the Darjeeling-Sikkim Himalaya (Patra & Saha, 2018).

Arc parallel extension is a significant component of the active deformation of the Himalaya. The arc parallel extension is manifested through arc perpendicular normal faults and arc parallel strike-slip faults (Styron, Taylor, & Murphy, 2011). It is observed that the slip directions along the fault plane are parallel to the Himalayan arc for active normal and strike-slip faults. This observation indicates an arc parallel extension in the Himalaya (Jessup, Newell, Cottle, Berger, & Spotila, 2008; Li & Yin, 2008; Murphy & Copeland, 2005; Murphy, Saylor, & Ding, 2009; Nakata, 1989). Although arc parallel extension is suggested to be along with the MCT (Hodges, Wobus, Ruhl, Schildgen, & Whipple, 2004), the prevalent active structures in the north of MFT are accommodating arc parallel extension. Several

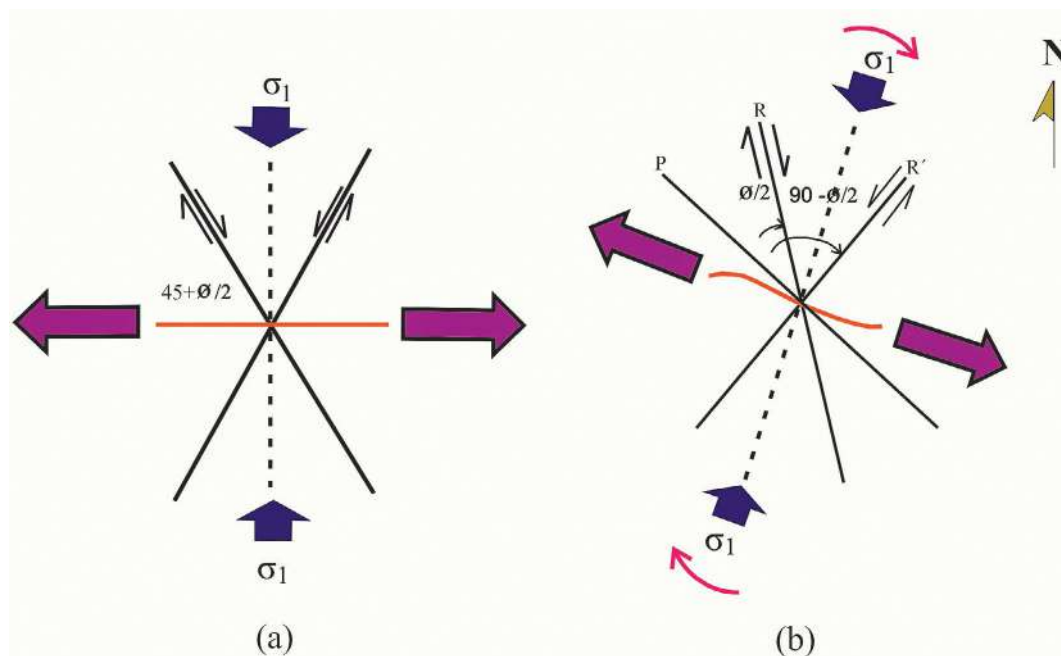


**FIGURE 12** (a) Pure shear model by Coulomb and Anderson (Sylvester, 1988). The N-S compression and associated E-W extension are shown (b) Reidal model for right simple shear. P and R fractures are synthetic and R' fracture is antithetic. The right simple shear is interpreted in terms of oblique convergence of Indian plate—see text for details

models explain the Himalayan arc parallel extension and strike-slip faulting: lateral extrusion of Tibet, oroclinal bending of Himalaya, radial spreading of Tibet and Himalaya, and oblique convergence between India and Himalaya. However, the geologic evidence of the arc parallel extension does not validate all the propositions made by the models as such. Only the oblique convergence model explains that the arc-parallel extension may be associated with arc subparallel strike-slip faulting. Towards the eastern Himalayan syntaxis, the oblique convergence and the clockwise rotation of the Indian plate might have resulted in a stress regime for the development of arc subparallel dextral strike-slip faults (Allmendinger, Reilinger, & Loveless, 2007; Shen, Lu, Wang, & B'urgmann, 2005; Styron et al., 2011).

The present area of study is bounded by two arc-perpendicular or arc-subparallel strike-slip faults: Kopili Fault in the west and Bomdila Fault in the east (Figure 1b). Palaeostress analysis from the joint data of the Gondwana and Siwalik sequences of the present area depicts a ~N-S extension for the Lower Gondwana Miri Formation representing a pre-Himalayan extension. Himalayan compression is reflected through two compression directions NW and NE. After the development of MBT-2, ~E-W extension represents active Himalayan deformation of arc-parallel extension north of MFT. If the arc-parallel extension is coupled with the model of oblique convergence and clockwise rotation of the Indian plate, a stress regime can be interpreted for the formation of Kopili and Bomdila faults in the region in phases (Figure 12; Goswami, Baruah, et al., 2020; Goswami, Mahanta, et al., 2020). Published age  $^{40}\text{Ar}/^{39}\text{Ar}$  dating of micas and (U-Th)/He dating of apatite from the Ama Drime Massif in southern Tibet suggests inception of arc-parallel extension in Himalaya at 13–12 Ma and this age coincides with the cessation of activity along with MCT and south Tibet Detachment (STD) locally (Jessup et al., 2008; Kali et al., 2010). It is difficult to assign the same age for extension in the Himalayan arc in the north of MFT. This is because the magnetostratigraphic age of deposition of Lower Siwalik sediments in Arunachal Himalaya is reported to be ~13 Ma and the youngest magnetostratigraphic age reported from the area is ~2 Ma (Chirouze et al., 2013; Gautam, Ulak, Paudyal, Gyawali, & Bhandari, 2012). On the other hand, there are several evidences of strike-slip offset of geomorphic features along the Bomdila Fault (Sharma et al., 2018). Therefore, the arc parallel extension is an active deformation phase in the Himalayan foreland in the north of MFT.

## 8 | CONCLUSIONS

Brittle deformation in the Gondwana and Siwalik sequence of the western Arunachal sub-Himalaya reveal meso-scale faults with eight slip senses: (a) top-to-NW (up) (F1) (b) top-to-NE (up) (F2) (c) top-to-SE (down) (F3) (d) top-to-NE (down) (F4) (e) top-to-SW (down) (F5) (f) top-to-SW (up) (F6) (g) top-to-SE (up) (F7) and (h) top-to-NW (down) (F8). Four varieties of joint sets are recorded from the area: two sets of inclined joints (a) ~NW-SE (J1) and (b) ~E-W joints (J2);

two sets of subvertical joints (c) WNW directed (J3) and (d) NNE directed (J4).

Slip senses of the meso-scale faults may be related to regional extension or compression. However, the faults may also indicate a local stress regime. F2 and F6 may represent NE- or NW-directed compressional event. F4 and F8 faults are recorded from the Miri Formation and may be linked to NNW-directed extensional tectonics. Therefore, it is also not possible to conclude that the sense of slip of all meso-scale faults reveals the Himalayan compressional stress regimes.

Palaeostress analysis reveals three stages of deformation constrained from the joint data of the Gondwana and Siwalik sequences. The subvertical joint sets (J3) were formed by the NNW-directed extension of the pre-Himalayan origin. Therefore, the inherited extension-related brittle deformation is documented in the Lower Gondwana rocks. The inclined joint sets of Bichom and Bhareli formations (J1 and J2) reveal NW and NNE-directed compression of the Himalayan orogeny. The subvertical joint sets (J4) recorded in the Dafla and Subansiri formations of the Siwalik sequence reveal a ~EW-directed extension. The arc-parallel extension in the frontal Himalayan fold belt may be due to the oblique India-Asia convergence and clockwise rotation of the Indian plate. This extension phase may be responsible for the formation of the arc subparallel Bomdila and Kopili faults in the eastern Himalaya.

## ACKNOWLEDGEMENTS

We are grateful to Dr. A. K. Singh (Guest Editor) for inviting the present paper. T.K.G. and M.G. received financial assistance from International Geological Congress Secretariat, New Delhi (IGC-2020) (No.36th IGC-Sectt./ Field Trips/2018/20.29 dt.05.11.2018-NER001). CPDA grant (IIT Bombay) supported SM. BNM and HS are thankful to the Dy. Director General, GSI, NER, Shillong for the permission and logistics to carry out the work. We thank the journal editor and two anonymous journal reviewers for their insightful comments that helped to improve the paper.

## PEER REVIEW

The peer review history for this article is available at <https://publons.com/publon/10.1002/gj.4393>.

## DATA AVAILABILITY STATEMENT

The data that support the findings of this study are openly available from corresponding author on request.

## ORCID

Tapos K. Goswami  <https://orcid.org/0000-0003-4489-597X>

Mousumi Gogoi  <https://orcid.org/0000-0003-1319-9226>

Bashab N. Mahanta  <https://orcid.org/0000-0002-6546-1575>

Soumyajit Mukherjee  <https://orcid.org/0000-0003-2247-8526>

Mohamedharoon A. Shaikh  <https://orcid.org/0000-0002-5886-3007>

Upendra Baral  <https://orcid.org/0000-0002-0679-0950>

## REFERENCES

- Acharyya, S. K. (1980). Structural framework and tectonic evolution of the eastern Himalaya. *Himalayan Geology*, 10, 412–439.
- Allmendinger, R. W., Reilinger, R., & Loveless, J. (2007). Strain and rotation rate from GPS in Tibet, Anatolia, and the Altiplano. *Tectonics*, 26, TC3013.
- Anderson, E. M. (1905). The dynamics of faulting. *Edinburgh Geological Society Transactions*, 8, 387–402.
- Anderson, E. M. (1951). *The dynamics of faulting and dyke formation with application to Britain* (pp. 133–147). Edinburgh: Oliver & Boyd.
- Angelier, J. (1984). Tectonic analysis of fault slips data sets. *Journal of Geophysical Research*, 89, 5835–5848.
- Angelier, J. (1989). From orientation to magnitudes in palaeostress determinations using fault slip data. *Journal of Structural Geology*, 11, 37–50.
- Angelier, J. (1994). Fault slip analysis and paleostress reconstruction. *Continental Deformation*, 4, 101–120.
- Angelier, J., & Mechler, P. (1977). Sur une méthode graphique de recherche des contraintes principales également utilisable en tectonique et en séismologie: la méthode des dièdres droits. *Bulletin de la Société Géologique de France*, 7(19), 1309–1318.
- Baruah, S., & Kayal, J. (2013). State of tectonic stress in northeast India and adjoining south Asia region: An appraisal. *Bulletin of Seismological Society of America*, 103, 894–910. <https://doi.org/10.1785/O120110354>.
- Bhattacharya, S., & Nandy, S. (2007). Geology of the western Arunachal Himalaya in parts of Tawang and west Kameng districts, Arunachal Pradesh. *Journal of Geological Society of India*, 72, 199–207.
- Bhattacharyya, K., & Ahmed, F. (2016). Role of initial basin width in partitioning total shortening in the Lesser Himalayan fold-thrust belt: Insights from regional balanced cross-sections. *Journal of Asian Earth Sciences*, 116, 122–131.
- Bhattacharyya, K., Mitra, G., & Kwon, S. (2015). Geometry and kinematics of the Darjeeling–Sikkim Himalaya, India: Implications for the evolution of the Himalayan fold-thrust belt. *Journal of Asian Earth Sciences*, 113, 778–796.
- Bhusan, S. K., Bindal, C. M., & Aggarwal, R. K. (1991). Geology of Bomdila Group in Arunachal Pradesh. *Journal of Himalayan Geology*, 2, 207–214.
- Biswas, S. K. (1999). A review on the evolution of Rift Basins in India during Gondwana with special reference to western Indian Basins and their hydrocarbon prospects. *Proceedings of the Indian National Science Academy*, 65(3), 261–283.
- Biswas, T., Bose, N., Dutta, D., & Mukherjee, S. (2022). Arc-parallel shears in collisional orogens: Global review and paleostress analyses from the NW lesser Himalayan sequence (Garhwal region, Uttarakhand, India). *Marine and Petroleum Geology*. Advance online publication.
- Bose, N., & Mukherjee, S. (2019). Field documentation and genesis of back-structures in ductile and brittle regimes from the foreland part of a collisional orogen: Examples from the Darjeeling–Sikkim lesser Himalaya, India. *International Journal of Earth Science*, 108, 1333–1350.
- Bott, M. H. P. (1959). The mechanics of oblique slip faulting. *Geological Magazine*, 96, 109–117.
- Célerier, B. (1988). How much does slip on reactivated fault plane constrain the stress tensor? *Tectonics*, 7, 1257–1278.
- Chakrabarti, B. K. (2016). *Geology of the Himalayan belt: Deformation, metamorphism, stratigraphy* (pp. 1–248). Amsterdam: Elsevier.
- Chen, N. C., Dong, J. J., Yang, S. F., Chen, J., Li, Z., & Ni, N. (2014). Restoration of geometry and emplacement mode of the Permian mafic dike swarms in Keping and its adjacent areas of the Tarim Block, NW China. *Lithos*, 204, 73–82.
- Chirouze, F., Bernet, M., Huyghe, P., Erens, V., Dupont-Nivet, G., & Senebier, F. (2012). Detrital thermochronology and sediment petrology of the middle Siwaliks molasse along the Muksar Khola section in eastern Nepal. *Journal of Asian Earth Sciences*, 44, 94–106. <https://doi.org/10.1016/j.jseas.2011.01.009>.
- Chirouze, F., Dupont-Nivet, G., Huyghe, P., van der Beek, P., Chakraborty, T., Bernet, M., & Erens, V. (2012). Magnetostratigraphy of the Neogene Siwalik Group of far eastern Himalaya, Kameng section, Arunachal Pradesh, India. *Journal of Asian Earth Sciences*, 44, 117–135. <https://doi.org/10.1016/j.jseas.2011.05.016>.
- Chirouze, F., Huyghe, P., van der Beek, P., Chauvel, C., Chakraborty, T., Dupont Nivet, D., & Bernet, M. (2013). Tectonics, exhumation, and drainage evolution of the eastern Himalaya since 13 Ma from detrital geochemistry and thermochronology, Kameng River section, Arunachal Pradesh. *Geological Society of America Bulletin*, 125, 523–538.
- Coulomb, C. A. (1776). Essai sur une application des regles de maximis et minimis quelques problemes de statique, relatifs a l'architecture. *Memoires de Mathematique de l'Academie Royale de Science*, 7, 343–382.
- Davis, G. H., Reynolds, S. J., & Kluth, C. (2012). *Structural geology of rocks and regions*. Hoboken, NJ: Wiley.
- de Sarkar, S., Mathew, G., & Pandey, K. (2013). Arc parallel extension in Higher and lesser Himalayas, evidence from western Arunachal Himalaya, India. *Journal of Earth System Science*, 122, 715–727.
- DeCelles, P. G., Carrapa, B., Gehrels, G. E., Chakraborty, T., & Ghosh, P. (2016). Along-strike continuity of structure, stratigraphy, and kinematic history in the Himalayan thrust belt: The view from northeastern India. *Tectonics*, 35, 2995–3027. <https://doi.org/10.1002/2016TC004298>.
- Delvaux, D., & Sperner, B. (2003). New aspects of tectonic stress inversion with reference to the TENSOR program. *Geological Society, London, Special Publications*, 212(1), 75–100. <https://doi.org/10.1144/GSL.SP.2003.212.01.06>.
- Delvaux, D., Moëys, Rikkert, S., Gerco, P., Carole, Levi, K., Miroshnichenko, A., Ruzhich, V., & San'kov, V. (1997). Paleostress reconstructions and geodynamics of the Baikal region, Central Asia, Part 2. Cenozoic rifting. *Tectonophysics*, 282, 1–38. [http://doi.org/10.1016/S0040-1951\(97\)00210-2](http://doi.org/10.1016/S0040-1951(97)00210-2)
- Devachandra, M., Kundu, B., Catherine, J., Kumar, A., & Gahalaut, V. K. (2014). Global Positioning System measurements of crustal deformation across the frontal eastern Himalayan Syntaxis and seismic-hazard assessment. *Bulletin of the Seismological Society of America*, 104(3), 1518–1524.
- Ding, L., Zhong, D., Yin, A., Kapp, P., & Harrison, M. (2001). Cenozoic structural and metamorphic evolution of the eastern Himalayan syntaxis (Namche Barwa). *Earth and Planetary Science Letters*, 192, 423–438.
- Doblas, M. (1998). Slickenside kinematic indicators. *Tectonophysics*, 295, 187–197.
- Dutta, D., Biswas, T., & Mukherjee, S. (2019). Arc-parallel compression in the NW Himalaya: evidence from structural and palaeostress studies of brittle deformation from the clasts of the upper Siwalik, Uttarakhand, India. *Journal of Earth System Science*, 128, 125.
- Fossen, H. (2016). *Structural geology* (2nd ed., p. 463). Cambridge: Cambridge University Press.
- Gautam, P., Ulak, P. D., Paudyal, K. N., Gyawali, B. R., & Bhandari, S. (2012). Magnetostratigraphic dating of the prime-time sedimentary record of Himalayan tectonics and climate: New age constraints (13–10 Ma) from the Siwaliks of the Tinau Khola north section, Nepal. *Geophysical Journal International*, 190, 1378–1392. <https://doi.org/10.1111/j.1365-246X.2012.05568.x>.
- Goswami, S. B., Bhowmik, S., & Dasgupta, S. (2009). Petrology of a non-classical Barrovian inverted metamorphic sequence from the western Arunachal Himalaya, India. *Journal of Asian Earth Sciences*, 36, 390–406.
- Goswami, S. B., Bhowmik, S., Dasgupta, S., & Pant, N. (2014). Burial of thermally perturbed Lesser Himalayan mid-crust: Evidence from petrochemistry and P-T estimation of the western Arunachal Himalaya, India. *Lithos*, 208–209, 298–311.
- Goswami, T. K., Baruah, S., Mahanta, B. N., Kalita, P., & Borah, P. (2020). Thrust shear sense and shear zone fabrics in higher Himalaya, Siyom valley, eastern Arunachal Himalaya, India. *Journal of Geological Society of India*, 96, 447–457.

- Goswami, T. K., Bezbaruah, D., Mukherjee, S., Sarmah, R. K., & Jabeed, S. (2018). Structures and morphotectonic evolution of the frontal fold-thrust belt, Kameng river Section, Arunachal Himalaya, India. *Journal of Earth System Science*, 127(88), 1–11.
- Goswami, T. K., Mahanta, B. N., Mukherjee, S., Syngai, B. R., & Sarmah, R. K. (2020). Orogen transverse structures in the eastern Himalaya: Dextral Riedel shear along the Main Boundary Thrust in the Garu-Gensi area (Arunachal Pradesh, India), implication in hydrocarbon geoscience. *Marine and Petroleum Geology*, 114, 104242. <https://doi.org/10.1016/j.marpetgeo.2020.104242>.
- GSI. (2010). *Geology and Mineral Resources of Arunachal Pradesh*, (Vol. 30, 54p). Shillong: Geological Survey of India.
- Hancock, P. L. (1985). Brittle microtectonics: principles and practice. *Journal of Structural Geology*, 7, 437–457.
- Hodges, K., Wobus, C., Ruhl, K., Schildgen, T., & Whipple, K. (2004). Quaternary deformation, river steepening and heavy precipitation at the front of the higher Himalayan ranges. *Earth and Planetary Science Letters*, 220, 379–389.
- Hodges, K. V. (2000). Tectonics of the Himalaya and southern Tibet from two perspectives. *Geological Society of America Bulletin*, 112(3), 324–350.
- Jayangondaperumal, R., Dubey, A. K., & Sen, K. (2010). Structural and magnetic fabric studies of recess structures in the western Himalaya: Implications for 1905 Kangra earthquake. *Journal of Geological Society of India*, 75, 225–238.
- Jayangondaperumal, R., Thakur, V. C., Jovivek, V., Rao, P. S., & Gupta, A. K. (2018). *Active tectonics of Kumaun and Garhwal Himalaya* (pp. 61–78). Singapore: Springer.
- Jessup, M. J., Newell, D. L., Cottle, J. M., Berger, A. L., & Spotila, J. A. (2008). Orogen parallel extension and exhumation enhanced by denudation in the Trans-Himalayan Arun River gorge, Ama Drime Massif, Tibet-Nepal. *Geology*, 36(7), 587–590.
- Kali, E., Leloup, P. H., Arnaud, N., Mahéo, G., Liu, D., Boutonnet, E., ... Li, H. (2010). Exhumation history of the deepest central Himalayan rocks, Ama Drime range: Key pressure-temperature-deformation-time constraints on orogenic models. *Tectonics*, 29, TC2014. <https://doi.org/10.1029/2009TC002551>.
- Kayal, J. R. (1996). Earthquake source process in northeast India: A review. *Journal of Himalayan Geology*, 17, 53–69.
- Kayal, J. R., Arefiev, S. S., Baruah, S., Tatevossian, R., Gogoi, N., Sanoujam, M., ... Borah, D. (2010). The 2009 Bhutan and Assam felt earthquakes (Mw 6.3 and 5.1) at the Kopili fault in the northeast Himalaya region. *Geomatics, Natural Hazards and Risk*, 1, 273–281.
- Keary, P., Klepeis, K. A., & Vine, F. J. (2009). *Global tectonics* (p. 307). Chichester: John Wiley.
- Kumar, G. (1997). *Geology of Arunachal Pradesh* (p. 217). Bangalore: Geological Society of India.
- Li, D., & Yin, A. (2008). Orogen-parallel, active left-slip faults in the eastern Himalaya: Implications for the growth mechanism of the Himalayan Arc. *Earth and Planetary Science Letters*, 274, 258–267.
- Liang, M., Peng, S., Du, W., & Lu, Y. (2018). Tectonic stress estimation from ultrasonic borehole image logs in a coal bed methane well, northeastern Qinshui Basin, China. *Journal of Natural Gas Science and Engineering*, 52, 44–58. <https://doi.org/10.1016/j.jngse.2018.01.021>.
- Mahanta, B. N., Sarmah, R. K., & Goswami, T. K. (2019). Elucidation of provenance, palaeoclimate and tectonic setting of the Gondwana sandstones of Arunachal Himalayas. *Journal of Geological Society of India*, 94(3), 260–266. <https://doi.org/10.1007/s12594-019-1305-7>.
- Mahanta, B. N., Sekhose, K., Goswami, T. K., Vitso, V., Sarmah, R. K., Kumar, A., & Kumar, R. (2021). Depositional setup of the faunal coal balls from Bichom formation of lower Gondwana Group of Arunachal Himalaya: Insights from EPMA and Raman spectroscopy. *Journal of Sedimentary Environments*, 6, 159–168. <https://doi.org/10.1007/s43217-020-00042>.
- Mahanta, B. N., Syngai, B. R., Sarmah, R. K., Goswami, T. K., & Kumar, A. (2020). Geochemical signatures of Lower Gondwana sandstones of eastern Arunachal Himalayas, India: Implications for tectonic setting, provenance and degree of weathering. *Russian Journal of Earth Science*, 20, 3–11. <https://doi.org/10.2205/2020ES000698>.
- Mahato, S., Mukherjee, S., & Bose, N. (2019). Documentation of brittle structures (back shear and arc-parallel shear) from Sategal and Dhanaulti regions of the Garhwal Lesser Himalaya (Uttarakhand, India). In S. Mukherjee (Ed.), *Tectonics and structural geology: Indian context* (pp. 411–424). Cham: Springer International Publishing.
- Mandl, G. (2005). *Rock joints: The mechanical genesis*. Heidelberg: Springer. <https://doi.org/10.1007/b137623>.
- Marrett, R., & Allmendinger, R. W. (1990). Kinematic analysis of fault-slip data. *Journal of Structural Geology*, 12, 973–986.
- Maurya, D. M., Shaikh, M. A., & Mukherjee, S. (2021). Comment on “Structural attributes and paleostress analysis of Quaternary landforms along the Vigodi Fault (VF) in western Kachchh region. Quaternary International <https://doi.org/10.1016/j.quaint.2020.07.038>”. *Quaternary International*, 601, 143–147. <https://doi.org/10.1016/j.quaint.2021.04.029>.
- Morely, C. K. (2017). The impact of multiple extension events, stress rotation and inherited fabrics on normal fault geometries and evolution in the Cenozoic rift basins of Thailand. *Geological Society London, Special Publications*, 439(1), 413–445.
- Mukherjee, S., Bose, N., Ghosh, R., Dutta, D., Misra, A. A., Kumar, M., ... Limaye, M. (2019). *Structural geological atlas*. Singapore: Springer Nature.
- Mukherjee, S., & Chakraborty, M. (2020). 3D-slip analyses of listric faults with ideal geometries. *Marine and Petroleum Geology*, 112, 104092. <https://doi.org/10.1016/j.marpetgeo.2019.104092>.
- Mukherjee, S., & Koyi, H. A. (2010a). Higher Himalayan Shear Zone, Sutlej section: Structural geology and extrusion mechanism by various combinations of simple shear, pure shear and channel flow in shifting modes. *International Journal of Earth Sciences*, 99, 1267–1303.
- Mukherjee, S., & Koyi, H. A. (2010b). Higher Himalayan Shear Zone, Zaskar Indian Himalaya: Microstructural studies and extrusion mechanism by a combination of simple shear & channel flow. *International Journal of Earth Science*, 99, 1083–1110.
- Mukherjee, S., Puneekar, J., Mahadani, T., & Mukherjee, R. (2015). A review on intrafolial folds and their morphologies from the detachments of the western Indian Higher Himalaya. In S. Mukherjee & K. F. Mulchrone (Eds.), *Ductile shear zones: From micro- to macro-scales* (pp. 182–205). New Jersey: Wiley Blackwell.
- Mukhopadhyay, B., Riguzzi, F., Mullick, M., & Sengupta, D. (2020). The strain rate and moment deficit along Indian Plate boundary: A tool for estimation of earthquake hazard. *Indian Journal of Geoscience*, 74, 1–21.
- Mukul, M. (2000). The geometry and kinematics of the Main Boundary Thrust and related neotectonics in the Darjiling Himalayan Fold-and-Thrust belt, west Bengal, India. *Journal of Structural Geology*, 22, 1261–1283.
- Murphy, M. A., & Copeland, P. (2005). Transtensional deformation in the central Himalaya and its role in accommodating growth of the Himalayan orogen. *Tectonics*, 24, TC4012. <https://doi.org/10.1029/2004TC001659>.
- Murphy, M. A., Saylor, J. E., & Ding, L. (2009). Late Miocene topographic inversion in southwest Tibet based on integrated paleoelevation reconstructions and structural history. *Earth and Planetary Science Letters*, 282, 1–9.
- Nakata, T. (1989). Active faults of the Himalaya of India and Nepal. *Geological Society of America Special Papers*, 232, 243–264. <https://doi.org/10.1130/spe232-p243>.
- Nemcok, M., & Lisle, R. J. (1995). A stress inversion procedure for poly-phase fault/slip data sets. *Journal of Structural Geology*, 17, 1445–1453. [https://doi.org/10.1016/0191-8141\(95\)00040-K](https://doi.org/10.1016/0191-8141(95)00040-K).
- Pandey, A., Jayangondaperumal, R., Hetenyi, G., Rao, P. S., Singh, I., Srivastava, P., & Srivastava, H. B. (2021). Establishing primary surface rupture evidence and magnitude of the 1697 CE Sadiya earthquake at the eastern Himalayan Frontal thrust, India. *Scientific Reports*, 11, 879. <https://doi.org/10.1038/s41598-020-79571-w>.

- Passchier, C. W., & Trouw, R. A. J. (2005). *Microtectonics* (2nd ed.). Heidelberg: Springer.
- Patel, R. C., Singh, P., & Lal, N. (2015). Thrusting and back-thrusting as post-emplacement kinematics of the Almora klippe: insights from low temperature thermochronology. *Tectonophysics*, *653*, 41–51.
- Patra, A., & Saha, D. (2018). Stress regime changes in the main boundary thrust zone, eastern Himalaya, decoded from fault-slip analysis. *Journal of Structural Geology*, *120*, 29–47.
- Pearson, O. M., & DeCelles, P. G. (2005). Structural geology and regional tectonic significance of the Ramgarh thrust, Himalayan fold-thrust belt of Nepal. *Tectonics*, *24*, 1–26.
- Rajendran, K., Parameswaran, R. M., & Rajendran, C. P. (2017). Seismotectonic perspectives of the Himalayan arc and contiguous areas: Inferences from past and recent earthquakes. *Earth Science Reviews*, *173*, 1–30.
- Ray, S. K. (1995). Lateral variation in geometry of thrust planes and its significance, as studied in the Shumar allochthon, Lesser Himalayas, eastern Bhutan. *Tectonophysics*, *249*, 125–139.
- Ray, S. K., Bandyopadhyay, B. K., & Razdan, R. K. (1989). Tectonics of a part of the Shumar allochthon in eastern Bhutan. *Tectonophysics*, *169*, 51–58.
- Roberts, J. C. (1975). Jointing and minor tectonics of the S. Crop of the south Wales Coalfield between Machen and Bridgend. *Geological Journal*, *10*(2), 147–160.
- Saha, D. (2013). Lesser Himalayan sequences in eastern Himalaya and their deformation: implications for Paleoproterozoic tectonic activity along the northern margin of India. *Geoscience Frontier*, *4*, 289–304.
- Sarma, J. N., & Sharma, S. (2018). Neotectonic activity of the Bomdila Fault in northeastern India from geomorphological evidences using remote sensing and GIS. *Journal of Earth System Science*, *127*, 113. <https://doi.org/10.1007/s12040-018-1008-2>.
- Sarma, K. P., Bhattacharyya, S., Nandy, S., Konwar, P., & Mazumdar, N. (2014). Structure, stratigraphy and magnetic susceptibility of Bomdila Gneiss, western Arunachal Himalaya, India. *Journal of Geological Society of India*, *84*, 544–554.
- Shah, J., Srivastava, D. C., & Joshi, S. (2012). Sinistral transpression along the main boundary thrust in Amritpur area, southeastern Kumaun Himalaya. *Tectonophysics*, *532–535*, 258–270. <https://doi.org/10.1016/j.tecto.2012.02.012>.
- Shaikh, M. A., Maurya, D., Mukherjee, S., Vanik, N., Padmalal, A., & Chamyal, L. (2020). Tectonic evolution of the intra-uplift Vigodi-Gugriana-Khirastra-Netra Fault System in the seismically active Kachchh rift basin, India: Implications for the western continental margin of the Indian plate. *Journal of Structural Geology*, *140*, 104124. <https://doi.org/10.1016/j.jsg.2020.104124>.
- Sharma, S., Sarma, J. N., & Baruah, S. (2018). Dynamics of Mikir hills plateau and its vicinity: Inferences on Kopili and Bomdila Faults in northeastern India through seismotectonics, gravity and magnetic anomalies. *Annals of Geophysics*, *61*, 3. <https://doi.org/10.4402/ag-7516>.
- Shen, Z., Lu, J., Wang, M., & Burgmann, R. (2005). Contemporary crustal deformation around the southeast borderland of the Tibetan plateau. *Journal of Geophysical Research*, *110*, B11409.
- Simón, J. L. (2019). Forty years of paleostress analysis: Has it attained maturity? *Journal of Structural Geology*, *125*, 124–133. <https://doi.org/10.1016/j.jsg.2018.02.011>.
- Simón, J. L., Arlegui, L. E., Liesa, C. L., & Maestro, A. (1999). Stress perturbations registered by jointing near strike-slip, normal and reverse faults. Examples from the Ebro Basin (Spain). *Journal of Geophysical Research*, *104*(B7), 15141–15153.
- Singh, I., Pandey, A. R., Mishra, R. L., Rao, S. P., Vrice, A., Jayagondaperumal, R., & Srivastava, V. (2021). Evidence of the 1950 great Assam earthquake surfacebreak along the Mishmi Thrust at Namche Barwa Himalayan Syntaxis. *Geophysical Research Letters*, *48*(11), 1–10. <https://doi.org/10.1029/2020GL090893>.
- Singh, P., & Patel, R. C. (2017). Post-emplacement kinematics and exhumation history of the Almora klippe of the Kumaun–Garhwal Himalaya, NW India: Revealed by fission track thermochronology. *International Journal of Earth Science*, *106*(6), 2189–2202.
- Singh, P., & Patel, R. C. (2021). Miocene development of the Main Boundary Thrust and Ramgarh Thrust, and exhumation of lesser Himalayan rocks of the Kumaun–Garhwal region, NW-Himalaya (India): Insights from fission track thermo chronology. *Journal of Asian Earth Sciences*, *224*, 104987. <https://doi.org/10.1016/j.jseae.2021.104987>.
- Singh, R. K. B., & Gururajan, N. S. (2011). Microstructures in quartz and feldspars of the Bomdila Gneiss from western Arunachal Himalaya, northeast India: Implications for the geotectonic evolution of the Bomdila mylonitic zone. *Journal of Asian Earth Sciences*, *6*, 1163–1178.
- Singh, R. K. B., Singh, A. K., Sen, K., & Sangode, S. J. (2017). Detection of a weak late-stage deformation event in granitic gneiss through anisotropy of magnetic susceptibility: Implications for tectonic evolution of the Bomdila Gneiss in the Arunachal lesser Himalaya, northeast India. *Geological Magazine*, *154*(3), 476–490.
- Singh, T., & Singh, P. (1983). Late early eocene larger foraminiferids from Siang district, Arunachal Pradesh, India and their geological significance. *Geoscience Journal*, *4*(2), 141–156.
- Sperner, B., & Zweigel, P. (2010). A plea for more caution in fault-slip analysis. *Tectonophysics*, *482*, 29–41.
- Srivastava, H. B., Srivastava, V., Srivastava, R. K., & Singh, C. K. (2011). Structural analyses of the crystalline rocks between Dirang and Tawang, west Kameng District, Arunachal Himalaya. *Journal of the Geological Society of India*, *78*, 45–56.
- Srivastava, V., Mukul, M., & Barnes, J. B. (2016). Main frontal thrust deformation and topographic growth of the Mohand Range, northwest Himalaya. *Journal of Structural Geology*, *93*, 131–148.
- Srivastava, V., Mukul, M., Barnes, J. B., & Mukul, M. (2018). Geometry and kinematics of Main Frontal thrust-related fault propagation folding in the Mohand Range, northwest Himalaya. *Journal of Structural Geology*, *115*, 1–18.
- Styron, R. H., Taylor, M. H., & Murphy, M. A. (2011). Oblique convergence, arc-parallel extension, and the role of strike slip faulting in the High Himalaya. *Geosphere*, *7*(2), 582–596.
- Sylvester, A. G. (1988). Strike-slip faults. *Geological Society of America*, *100*, 1666–1703.
- Thakur, V. C., & Pandey, A. K. (2004). Late quaternary tectonic evolution of Dun in fault bend/propagated fold system, Garhwal Sub-Himalaya. *Current Science*, *87*, 1567–1576.
- Tranos, M. D. (2015). TR method (TRM): A separation and stress inversion method for heterogeneous fault-slip data driven by Andersonian extensional and compressional stress regimes. *Journal of Structural Geology*, *79*, 57–74.
- Tranos, M. D. (2018). The use of Stress Tensor Discriminator Faults in separating heterogeneous fault-slip data with best-fit stress inversion methods. II. Compressional stress regimes. *Journal of Structural Geology*, *107*, 153–162.
- Twiss, R. J., & Moores, E. M. (2007). *Structural Geology* (53p). New York: WH Freeman and Company.
- Twiss, R. J., & Unruh, J. R. (1998). Analysis of fault slip inversions: Do they constrain stress or strain rate? *Journal of Geophysical Research*, *103*, 12205–12222.
- Vanik, N., Shaikh, M., Mukherjee, S., Maurya, M., & Chamyal, L. S. (2018). Post-deccan trap stress reorientation under transpression: Evidence from fault slip analyses from SW Saurashtra, western India. *Journal of Geodynamics*, *121*, 9–19. <https://doi.org/10.1016/j.jog.2018.06.004>.
- Wallace, R. E. (1951). Geometry of shearing stress and relation to faulting. *The Journal of Geology*, *59*, 118–130. <http://doi.org/10.1086/625831>

- Wesnowsky, S. G., Kumar, S., Mahindra, R., & Thakur, V. C. (1999). Uplift and convergence along the Himalayan frontal thrust of India. *Tectonics*, 18, 967–976.
- Winsor, C. N. (1979). The correlation of fracture directions with sediment anisotropy in folded rocks of the Delamerian fold belt at Port Germein gorge, south Australia. *Journal of Structural Geology*, 1, 245–254.
- Wopfner, H., & Jin, X. (2009). Pangea Megasequences of Tethyan Gondwana-margin reflect global changes of climate and tectonism in Late Palaeozoic and Early Triassic times-A review. *Palaeoworld*, 18(2), 169–192.
- Yamaji, A., Otsubo, M., & Sato, K. (2006). Paleostress analysis using the Hough transform for separating stresses from heterogeneous fault slip data. *Journal of Structural Geology*, 28, 980–990.
- Yin, A. (2006). Cenozoic tectonic evolution of the Himalayan orogeny as constrained by along strike variation of structural geometry, exhumation history, and foreland sedimentation. *Earth-Science Reviews*, 76, 1–131.
- Yin, A., Dubey, C. S., Kelty, T. K., Gehrels, G. E., Chou, C. Y., Grove, M., & Lovera, O. (2006). Structural evolution of the Arunachal Himalaya and implications for asymmetric development of the Himalayan orogen. *Current Science*, 90, 195–206.
- Yin, A., Dubey, C. S., Webb, A. A. G., Kelty, T. K., Grove, M., Gehrels, G. E., & Burgess, W. P. (2010a). Geological correlation of the Himalayan orogen and Indian craton: Part 1. Structural geology, U-Pb zircon geochronology, and tectonic evolution of the Shillong Plateau and its neighboring regions in NE India. *Geological Society of America Bulletin*, 122, 336–359.
- Yin, A., Dubey, C. S., Webb, A. A. G., Kelty, T. K., Grove, M., Gehrels, G. E., & Burgess, W. P. (2010b). Geologic correlation of the Himalayan orogen and Indian craton: Part 2. Structural geology, geochronology and tectonic evolution of the eastern Himalaya. *Geological Society of America Bulletin*, 122, 360–395.
- Žalohar, J., & Vrabec, M. (2008). Combined kinematic and paleostress analysis of fault slip data: the multiple-slip method. *Journal of Structural Geology*, 30, 1603–1613.
- Zalohar, J. (2015). On a new law of faulting along tectonic wedges: Cosserat explanation of the preferred (paleo) stress states in the Earth's crust. *Journal of Structural Geology*, 77, 107–125. <https://doi.org/10.1016/j.jsg.2015.05.016>.
- Žalohar, J., & Vrabec, M. (2007). Paleostress analysis of heterogeneous fault-slip data: the Gauss 730 method. *Journal of Structural Geology*, 29, 1798–1810.
- Zalohar, J., & Vrabec, M. (2010). Kinematics and dynamics of fault reactivation: The Cosserat approach. *Journal of Structural Geology*, 32(1), 15–27. <https://doi.org/10.1016/j.jsg.2009.06.008>.

**How to cite this article:** Goswami, T. K., Gogoi, M., Mahanta, B. N., Mukherjee, S., Saikia, H., Shaikh, M. A., Kalita, P., Baral, U., & Sarmah, R. K. (2022). Brittle tectonics in the western Arunachal Himalayan frontal fold belt, northeast India: Change in stress regime from pre-collisional extension to collisional compression. *Geological Journal*, 57(12), 5019–5038. <https://doi.org/10.1002/gj.4393>